ChemComm
Chemical Communications

Accepted Manuscript

This article can be cited before page numbers have been issued, to do this please use: A. Charisiadis, V. Nikolaou, E. Nikoloudakis, K. Ladomenou, G. Charalambidis and A. G. Coutsolelos, *Chem. Commun.*, 2025, DOI: 10.1039/D4CC06655C.

ROYAL SOCIETY OF CHEMISTRY

rsc.li/chemcomm

View Article Online
DOI: 10.1039/D4CC06655C

FEATURE ARTICLE

Metalloporphyrins in Bio-Inspired Photocatalytic Conversions

Asterios Charisiadis,[a] Vasilis Nikolaou,[b] Emmanouil Nikoloudakis,[c,d] Kalliopi Ladomenou,*[e] Georgios Charalambidis*[f] and Athanassios G. Coutsolelos*[c,d]

Received 00th January 20xx,
Accepted 00th January 20xx

DOI: 10.1039/x0xx00000x

Numerous natural systems contain porphyrin derivatives that facilitate important catalytic processes; thus, developing biomimetic photocatalytic systems based on synthetic metalloporphyrins constitute a rapidly advancing and fascinating research field. Additionally, porphyrins are widely investigated in a plethora of applications due to their highly versatile structure, presenting advantageous photoredox, photophysical and photochemical properties. Consequently, such metallated tetrapyrrolic macrocycles feature prominently as photosensitizers and catalysts in developing artificial photosynthetic systems that can store and distribute energy through fuel forming reactions. This Review highlights the advances in the field of metalloporphyrin-based biomimetic photocatalysis, and particularly targeting water splitting, including both hydrogen and oxygen evolution reactions, carbon dioxide reduction and alcohol oxidation. For each photocatalytic system different approaches are discussed, concerning either structural modifications of the porphyrin derivatives or the phase in which the process takes place, i.e. homogenous or heterogenous. The most important findings for each porphyrin-based photocatalytic reaction are presented and accompanied by the analysis of mechanistic aspects when possible. Finally, the perspectives and limitations are discussed, providing future guidelines for the development of highly efficient metalloporphyrin-based biomimetic systems towards energy and environmental applications.

1. Introduction

Porphyrins are one of few cases where a similar molecular framework is used in almost any imaginable application.[1-3] Porphyrin systems feature prominently in biomimetic photocatalysis due to their well-established chemistry and highly versatile structural properties.[4-7] Specifically, they are aromatic systems (18-π electrons) that present exceptional light-absorption properties, high thermal and chemical stability, and an efficient production of separated ion products upon irradiation. The porphyrin macrocycle is composed of four pyrrole units that are linked at their α-carbons through methine bridges, and can be easily modified by introducing a wide range of functional groups to their periphery.[8, 9] Furthermore, the inner core of these macrocyclic compounds can accommodate any transition metal ion, hence enhancing their photochemical and photoredox properties.[10]

What is more, many natural systems, such as heme, chlorophyll, cytochromes and peroxidases, contain tetrapyrrole skeletons, with multifaceted uses in oxygen and carbon dioxide (CO_2) transport, electron transfer, catalysis, and photosynthesis.[11-13] Those "pigments of life" play a key role in sustaining aerobic life on Earth;[14] thus being widely employed in systems dealing with some of the most pressing energy challenges in an environment-friendly and sustainable way. Metalloporphyrins have been recognized as ideal photosensitizers and catalytic units, based on their excellent light-harvesting properties and photocatalytic activity, respectively.[15-17] This Feature article focuses on recent progress in the emerging field of porphyrin-based artificial photosynthetic systems, capable of storing and distributing solar energy through fuel forming reactions.[18]

One of the most urgent scientific challenges targets the production of carbon-neutral energy by exploiting renewable sources, i.e. sunlight and water, due to the extensive depletion of fossil fuels and resulting global warming.[19] Artificial photosynthesis, and particularly photocatalytic water-splitting systems have attracted significant interest.[20] Such systems facilitate the conversion of photon energy to chemical energy,[21] by tackling different light-induced catalytic processes. Particularly, reduction of aqueous protons to form hydrogen (H_2) constitutes the reductive side of water splitting, and is one of the major strategies for solar energy conversion being widely investigated.[5, 22, 23] Another substantial strategy is the photocatalytic transformation of carbon dioxide into useful hydrocarbons, since no CO_2 emissions decrease is foreseen in the following years.[24, 25] The products of this reductive process can act either as fuels (methane or methanol) or valuable chemical substances (carbon monoxide, formic acid or formaldehyde). Notably, the water oxidation reaction is particularly challenging since efficient water oxidation catalysts are needed to accelerate the concomitant removal of four protons and four electrons, coupled with the formation of an O=O bond.[26, 27] Hence, the oxidative side of water splitting is considered the key step

[a] Instituto de Ciencia de Materiales de Madrid, Consejo Superior De Investigaciones Científicas, Sor Juana Inés de la Cruz, 3, Madrid, Spain.
[b] Chimie Et Interdisciplinarité, Synthèse, Analyse, Modélisation (CEISAM), CNRS UMR 6230, Nantes, France.
[c] Laboratory of Bioinorganic Chemistry, Department of Chemistry, University of Crete, Heraklion, Crete, Greece.
[d] Institute of Electronic Structure and Laser (IESL), Foundation for Research and Technology – Hellas (FORTH), Heraklion, Greece.
[e] Hephaestus Laboratory, School of Chemistry, Faculty of Sciences, Democritus University of Thrace, GR-65404 Kavala, Greece.
[f] Theoretical and Physical Chemistry Institute, National Hellenic Research Foundation, Athens, Greece.

View Article Online DOI: 10.1039/D4CC06655F

in both natural and artificial photosynthetic systems. Due to the high energetic barrier of this process, alternative catalytic reactions have also been targeted, with the most appealing being the oxidation of alcoholic organic compounds.[28] Importantly, such transformations offer a valuable strategy to exploit biomass, which is an alcohol-rich source, and produce high-valued carbonyl compounds.[29]

In this feature article we will focus on our group´s contributions in developing porphyrin-based assemblies towards biomimetic photocatalytic applications.[5] Additionally, some of the most important findings for each bio-inspired photocatalytic transformation will be discussed. In all cases two different approaches can be followed to achieve the catalytic processes, viz homogenous or heterogenous systems.[30] For all systems discussed herein, the solar-driven catalytic conversion is achieved by employing assemblies that contain metalloporphyrins acting either as photosensitizers or as catalysts. In the homogenous systems, the photosensitizer (PS) and catalyst (CAT) units are combined with a sacrificial electron acceptor (SEA: for the oxidative processes) or donor (SED: in both reduction reactions) (Scheme 1a, b).[31-34] The PS and CAT moieties can interact either through diffusion forces or via covalent bonding and have well-defined structures, making the determination of the mechanistic aspects easier.

The presence of a sacrificial agent along with the photodegradation of the PS and/or CAT units, constitute the main drawbacks of such systems. An elegant approach to overcome these issues concerns the adsorption of the photosensitizer and catalyst on semiconductor electrodes or nanoparticles (Scheme 1c, d).[35-38] In such heterogenous photochemical systems, the semiconducting nanoparticles facilitate the electron or hole transfer between the chromophore and catalytic entities to efficiently perform each corresponding process. What is more, the adsorption of both the PS and CAT entities on semiconducting surfaces minimizes their tendency to self-aggregate; hence increasing their stability. Heterogeneous catalytic assemblies further achieve enhanced photocatalytic efficiencies, since both structural and electronic aspects of the immobilized moieties (coordination number and environment, metal spin state, etc.) are altered through their interaction with the semiconducting substrate.

As discussed herein, metalloporphyrins have been extensively studied both as photosensitizers and catalysts for such bio-inspired catalytic processes. Water splitting is a two-part process involving both oxygen evolution and hydrogen production. While O_2 evolution is often considered the more energetically demanding step, H_2 evolution is equally critical, as it directly produces hydrogen gas—a clean and versatile fuel. This highlights the importance of understanding and optimizing hydrogen evolution systems, which will be the focus of the next section. Emphasis will be given to zinc-metallated porphyrins, which are among the most extensively studied photosensitizers in applications such as H_2 evolution and alcohol oxidation. Zn-porphyrins have proven to be exceptional light-harvesters, often being the main components of photosynthetic reaction center mimics as they efficiently promote charge separation processes.[39, 40] Additionally, examples of various metallated macrocycles acting as photocatalysts towards H_2 production will be presented. Regarding the transformation of CO_2 to valuable carbon-based products, iron-porphyrins are amongst the most efficient catalysts that have been developed thus far.[41] As far as water oxidation systems are concerned, porphyrins that contain different metal ion centres, namely Zn and Ru or Ni and Co, have been used either as photosensitizers[32, 38] or as catalysts,[42, 43] respectively. Finally, the perspectives and limitations are highlighted as they arise from our group´s work, providing future guidelines for the development of highly efficient biomimetic catalytic systems based on metalloporphyrin derivatives.

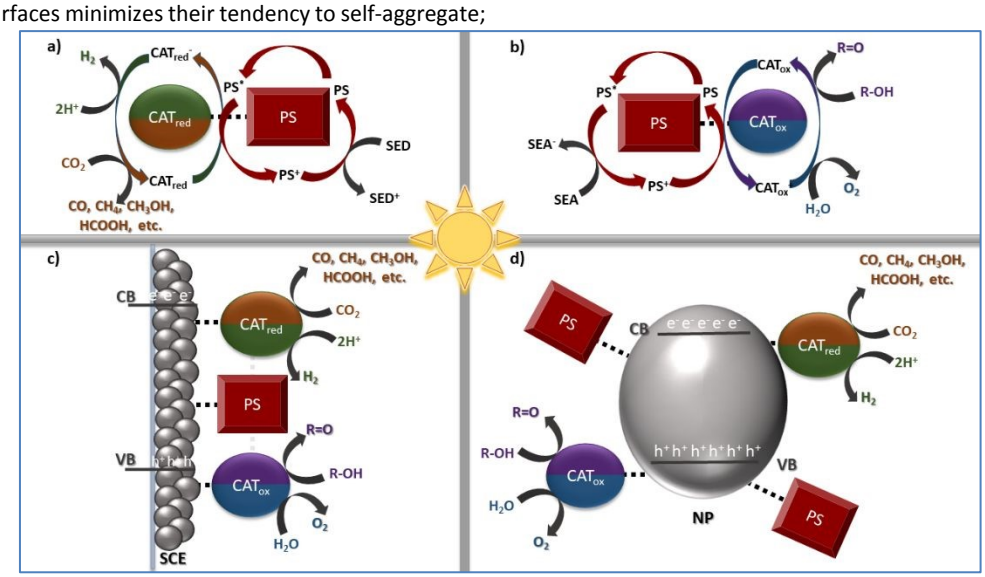

Scheme 1: Upper part: Simplified schematic representation of homogenous photocatalytic systems toward reduction of H^+ to H_2 or CO_2 to CO, CH_4, CH_3OH, HCOOH (a), and water or alcohol oxidation (b). PS: photosensitizer, CAT: catalyst, SEA: sacrificial electron acceptor and SED: sacrificial electron donor. Lower part: Simplified schematic representation of heterogenous photocatalytic systems by employing either a semiconducting electrode (c) or nanoparticles (d). PS: photosensitizer, CAT: catalyst, SCE: s emiconductor electrode, NP: nanoparticles, CB: conduction band and VB: valance band.

2. Photocatalytic hydrogen evolution

Photocatalytic hydrogen evolution is a process bioinspired by photosynthesis.[44] In natural photosynthesis, plants use chlorophyll to absorb sunlight and drive a series of reactions that convert water

and carbon dioxide into glucose and oxygen. Similarly, in photocatalytic hydrogen production, artificial photocatalysts absorb sunlight to initiate the splitting of water into hydrogen and oxygen.[45-48] Both processes aim to convert solar energy into a usable form of chemical energy. Conversely, artificial photocatalytic systems convert solar energy into H_2, a versatile and clean fuel that can be stored and later used in fuel cells or other applications.[19, 49] Both natural and artificial photosynthetic assemblies employ specific light-harvesting compounds, i.e. chlorophyll and photosensitizers respectively, capable of exciting electrons. This electron excitation is the critical step that provides the energy needed to break the chemical bonds in water, leading to hydrogen production. Ideal photosensitizers should meet several key requirements, including chemical stability, an appropriate band gap energy, favorable thermodynamic redox potentials, and high activity. Among the various types explored, porphyrins rank among the best due to their unique structure and similarity to natural systems.[46, 50-52]

Porphyrins form hybrid photocatalytic systems when combined with semiconductors.[5, 30, 53] Owing to their advantages—such as excellent light-harvesting capabilities, efficient photoinduced electron transfer, and structural versatility—they can serve multiple roles in photocatalytic hydrogen evolution systems. Particularly they can act as photosensitizers, photocatalysts, or catalysts. The photocatalytic process can be classified as either homogeneous or heterogeneous, depending on the phase in which the reaction occurs. Regarding the homogeneous systems, the well-defined structures of the individual components significantly aid in elucidating all mechanistic aspects of H_2 evolution. On the other hand, heterogeneous assemblies offer several advantages, such as the presence of semiconducting surfaces, which make them suitable for practical applications, such as solar fuel cells. A photochemical system requires a photosensitizer (PS), a sacrificial electron donor (SED) and a catalyst (Scheme 2).

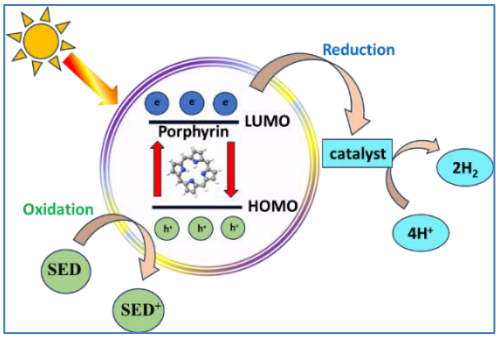

Scheme 2. Simplified scheme of half-cycle photochemical H_2 evolution.

For efficient hydrogen evolution, the conduction band (CB) or LUMO energy level must be sufficiently negative relative to the hydrogen evolution potential, while the valence band (VB) level or HOMO orbital must be more positive than the oxygen generation potential. This process requires a minimum energy input of 1.23 eV. Since most dyes, including porphyrins, absorb visible light in the range of 1.5 to 3.1 eV, they possess sufficient thermodynamic power to drive the water-splitting reaction.

The primary challenges are kinetics, arising from the difference in speed between the rapid charge separation (and recombination) procedure and the slow oxidation and reduction of water. Therefore, an essential element in any photochemical water-splitting cycle is the use of multi-electron catalysts. Such units can store electrons or positive charges produced by the photosystem and transfer them to the substrate through low-energy activation pathways. Considerable research is currently directed at developing more efficient catalysts for both water oxidation and hydrogen evolution.[54-57] Understanding the photophysics of photocatalytic components is crucial for designing assemblies that enhance hydrogen production and improve stability. Homogeneous catalysis can offer insights into the mechanisms behind light-driven reactions, contributing to the advancement of heterogeneous photocatalytic systems. Thus far, three major approaches were adopted by our group in photocatalytic H_2 evolution reaction (HER): (i) homogeneous photocatalytic systems, where porphyrins act as photosensitizers, (ii) self-assembled heterogeneous photocatalytic systems, and (iii) dye-sensitized heterogeneous photocatalytic systems (DSPs).

Since the late 1970s, numerous homogeneous photocatalytic hydrogen-evolution systems have been developed, revealing two distinct mechanistic behaviors: oxidative quenching and reductive quenching. These mechanisms depend on the direction of the initial electron transfer in the excited state: either from the photosensitizer to the catalyst (oxidative quenching) or from the sacrificial electron donor (SED) to the photosensitizer (reductive quenching). Coutsolelos and colleagues reported for the first time a bioinspired noble-metal free photocatalytic system based on water-soluble porphyrin PS and cobalt-based CAT. More specifically, our group synthesized water soluble porphyrins, both free-base (**TMPyP**) and metalated with zinc (**ZnTMPyP**), and studied their activity as PS in the presence of cobalt complexes such as cobaloxime (**Cat1**) (Fig. 1).[58]

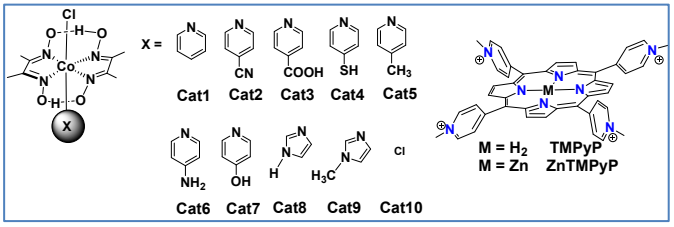

Fig. 1. Chemical structures of porphyrin-based photosensitizer and cobaloxime-based catalysts.

The system produces hydrogen under visible light irradiation (λ > 400 nm) in an acetonitrile-water (1:1) solution, using triethanolamine (TEOA) as SED, reaching a maximum turnover number (TON) of 280 after 25 hours. In a follow-up study, our group tested the activity of the same **ZnTMPyP** photosensitizer with various cobaloxime catalysts featuring different axial ligands (Fig. 1).[59] The catalysts were modified by incorporating diverse pyridine and imidazole axial ligands. Notably, the catalyst with N-methyl imidazole (**Cat9**) achieved the highest catalytic performance with a TON of 1135 after 50 hours of irradiation, while the imidazole ligand-based catalyst (**Cat8**) reached 565 TONs. Among the catalysts with pyridine axial ligands, those with electron-donating groups were more effective for hydrogen production. One of the main drawbacks of this type of homogenous system was its instability. To address this issue, we further improved it by employing heterogeneous photocatalysis.

A second approach concerns the use self-assembled porphyrin molecules designed to replicate the organized structures of

chlorophyll in photosynthesis. These self-assembled chromophores exhibit distinct properties compared to their monomeric counterparts, such as broader and intensified light absorption.[60-62] We synthesized a peptide nucleic acid (PNA)-porphyrin derivative, **PNA-TPP**[63] and a peptide-(Zn)porphyrin hybrid, **Fmoc-FF-(Zn)Por**[64] to study their self-assembly characteristics and catalytic activity for H_2 evolution (Fig. 2). Both conjugates form supramolecular architectures when exposed to a mixed solvent system using the "good-bad" solvent protocol. For **PNA-TPP**, spherical structures formed in a dichloromethane-ethanol (2:8) mixture (Fig. 2(a)). Under visible light irradiation in the presence of Pt nanoparticles, **PNA-TPP** achieved an H_2 production of 74.43 nmol over 4.5 hours. Control experiments with a mixed solution of 0.1 M ascorbic acid and 5 µM K_2PtCl_4 resulted in minimal H_2 production (12 nmol in 4.5 hours), indicating the effectiveness of the assembled nanostructure in light harvesting. The porphyrin-peptide hybrid **Fmoc-FF-(Zn)Por** self-assembled into nanospheres or fibrils, depending on the solvent system used. Nanospheres (Fig. 2(b)) formed when **Fmoc-FF-(Zn)Por** was dissolved in tetrahydrofuran (THF) and diluted in methanol (THF/MeOH, 2:8). Conversely, using a dichloromethane/heptane (1:1) mixture resulted in the formation of micrometer-long fibrils instead (Fig. 2(c)). By adjusting the solvent mixture, the same compound can self-assemble into two distinct nanostructures. When evaluated for their photocatalytic activity in HER, each morphology demonstrated varying levels of efficiency. The fibril-like nanostructures of **Fmoc-FF-(Zn)Por** showed the highest catalytic performance, achieving a maximum H_2 evolution rate of 1.96 mmol g^{-1} h^{-1} and remaining highly stable for over 400 hours under irradiation, with a maximum turnover number (TON) of 155. In contrast, the spherical nanostructures displayed minimal photocatalytic activity, reaching only 10 TONs after 360 hours of irradiation. Additionally, the catalytic efficiency of the amorphous solid was 17 TONs after 378 hours of irradiation, somewhat better than the spherical nanostructures but still significantly lower than the fibrillar nano-assemblies.

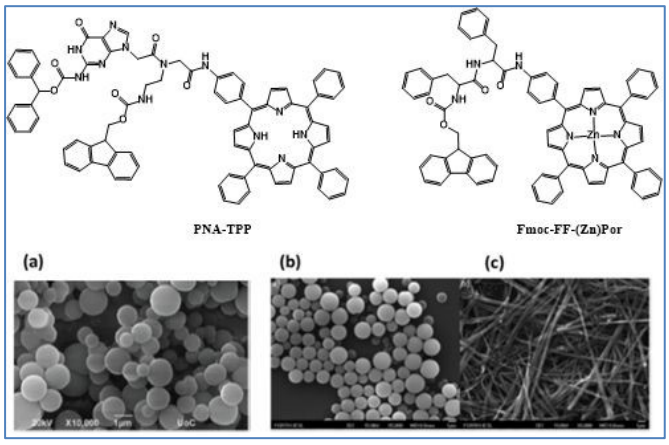

Fig. 2. Chemical nanostructures of self-assembled porphyrins and SEM images of (a) PNA-TPP CH_2Cl_2–EtOH, 2:8 (7 mM), (b) Fmoc-FF-(Zn)Por THF/MeOH, 2:8 (1 mM), (c) Fmoc-FF-(Zn)Por CH_2Cl_2/Hept, 1:1 (1 mM). Reproduced from ref. 63 with permission from Royal Society of Chemistry, copyright 2019.

Bai, Zhu, and colleagues investigated self-assembled porphyrin nanoleaves that effectively enhanced photochemical hydrogen evolution (Fig. 3).[65] A Pd(II)-tetra(4-carboxyphenyl)-porphyrin PdTCPP, was self-assembled in N,N-dimethylformamide (DMF) with the assistance of the surfactant 1-decanesulfonic acid through π-π interactions and hydrogen bonding. Both experimental data and theoretical calculations indicated the formation of a strong internal electric field, enabling the directional transport of photogenerated electrons and holes, and supporting efficient photocatalytic hydrogen production. Photocatalytic experiments were conducted under visible light irradiation (λ > 400 nm) with ascorbic acid as the sacrificial agent. After 5 hours of irradiation, the nanoleaves achieved a H_2 production rate of 9.9 mmol g^{-1} h^{-1} without additional cocatalysts, a rate 40 times higher than that of commercial PdTCPP powder (0.25 mmol g^{-1} h^{-1}). The nanoleaves also demonstrated excellent stability, maintaining a steady H_2 production rate over 100 hours of visible light exposure. This study highlights the significance of a long-range conjugated structure in enhancing photocatalytic performance in porphyrin assemblies.

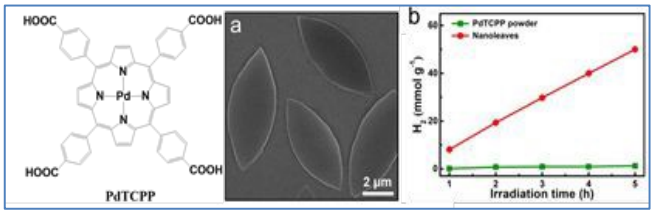

Fig. 3. Chemical structure of **PdTCPP**, (a) SEM image of nanoleaves, (b) photocatalytic H_2 production of the commercial **PdTCPP** powder and nanoleaves without cocatalysts. Reproduced from ref. 65 with permission from American Chemical Society, copyright 2022.

In a similar work, our group reported a noble-metal free Zn(II)-porphyrin derivative (**ZnTPP**) that was self-assembled into three distinct structures. Subsequently, those three different self-assemblies were studied as photosensitizers on the photocatalytic hydrogen evolution system in water (Fig. 4).[66] These structures were prepared with the "good-bad" solvent self-assembly protocol, maintaining the same "bad" solvent while varying the "good" solvent. This approach produced three different structural forms, each displaying unique catalytic activity for H_2 production in the presence of 5% w/w Pt nanoparticles as catalysts and ascorbic acid as a sacrificial electron donor. The octahedral form achieved the highest hydrogen evolution rate of 185.5 µmol g^{-1} h^{-1}. Additionally, the porphyrin could be recycled and reassembled into the optimal structure for H_2 production. This work demonstrates that simple porphyrin-based chromophores can be effectively optimized for photocatalytic hydrogen evolution through controlled self-organization in mixed solvent systems.

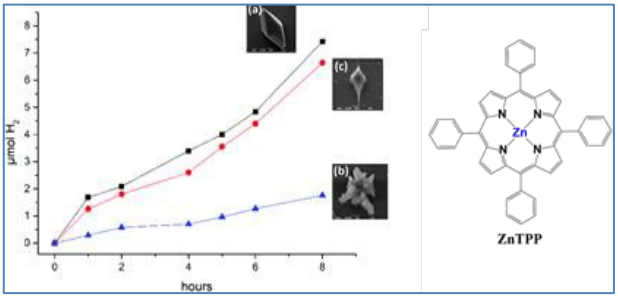

Fig. 4. Photocatalytic hydrogen production of **ZnTPP** with (a) octahedral (THF/MeOH 1:4), (b) "flower" ($CHCl_3$/MeOH 1:4), (c) "manta-ray" (Tol/MeOH 1:4), in the presence of Pt nanoparticles. Reproduced from ref. 66 with permission from Royal Society of Chemistry, copyright 2022.

An alternative approach for efficient H_2 production evolution is the dye-sensitized photocatalytic systems. In this kind of system TiO_2 nanoparticles act as a scaffold were a photosensitizer and a catalyst are adsorbed forming a heterogeneous photocatalyst. Numerous studies have explored various molecular photosensitizers and catalysts in TiO_2-based dye-sensitized systems.[67, 68] In addition, the deposition of Pt nanoparticles onto the TiO_2 semiconductor, results in highly efficient and stable systems towards H_2 evolution.[69-71] Coutsolelos and coworkers further advanced this approach by using porphyrin-based photocatalysts ameliorating the H_2 production of the system.[71] In a recent report, our group prepared two types of metallated porphyrin derivatives bearing carboxylic acids for the attachment onto Pt-TiO_2 nanoparticles.[72] In one variant, the carboxylic acid was attached via a three-carbon alkyl chain at the para-position of the phenyl ring (**M-Tc$_3$CP**, **M**=**Zn**, **Pd**, **Pt**) (Fig. 5).

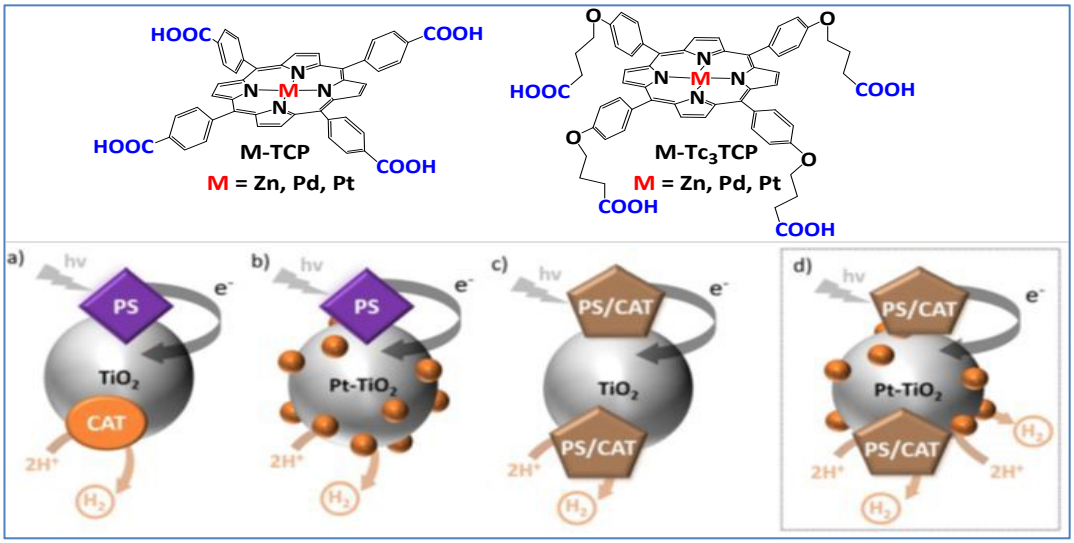

Fig. 5. Chemical structures of porphyrin molecules **M-TCP**, **M-Tc$_3$TCP** adsorbed onto TiO_2 nanoparticles, (a) **PS** and **CAT** on TiO_2 nanoparticles, (b) **PS** onto Pt-TiO_2 nanoparticles, (c) **PS-CAT** onto TiO_2 nanoparticles, (d) **PS-CAT** onto Pt-TiO_2 nanoparticles. Reproduced from ref. 72 with permission from Royal Society of Chemistry, copyright 2023.

In the other series, the carboxylic acid group was directly attached to the para-position of the four *meso*-phenyl rings (**M-TCP**, **M**=**Zn**, **Pd**, **Pt**). The photocatalytic performance of the porphyrin-based dye-sensitized photocatalysts was notably affected by the amount of porphyrin adsorbed onto the TiO_2 nanoparticles. Analysis of the optimal photocatalytic results for each system indicates that all **M-Tc$_3$TCP** derivatives outperform their **M-TCP** counterparts in terms of both stability and efficiency. However, **Zn-TCP** and **Zn-Tc$_3$TCP** showed nearly equivalent TONs and similar H_2 evolution rates, suggesting that the photocatalytic activity of Zn-porphyrin derivatives is unaffected by the type of anchoring group, verifying their role solely as photosensitizers. In contrast, both **Pd-Tc$_3$TCP** and **Pt-Tc$_3$TCP** demonstrated superior TONs and H_2 evolution rates compared to their respective **Pd-TCP** and **Pt-TCP** counterparts. Notably, **Pt-Tc$_3$CP** exhibited outstanding performance, achieving 11607 TONs and 458 mmol g^{-1} h^{-1} of H_2 evolution, far exceeding **Pt-TCP**, which reached 2525 TONs and 378 mmol g^{-1} h^{-1} of H_2. The enhanced efficiency of the **M-Tc$_3$CP** over the **M-TCP** derivatives may be due to their adsorption via four anchoring groups, which promotes a well-ordered self-assembly of the **M-Tc$_3$CP** structures. While all reported examples rely on a sacrificial donor, a dye-sensitized system would be more sustainable if dye regeneration were achieved through an oxidation reaction, potentially transforming abundant substrates into valuable products. This approach will be discussed in the following section on photocatalytic alcohol oxidation. While hydrogen evolution is a critical component of artificial photosynthesis for generating clean energy, another equally vital strategy focuses on mitigating carbon dioxide emissions through its transformation into valuable fuels and chemicals. This approach addresses the dual challenges of renewable energy production and environmental sustainability, which leads us to the next significant process in artificial photosynthesis: photocatalytic CO_2 reduction.

3. Photocatalytic CO_2 reduction

The reliance on fossil fuels as primary energy sources has led to widespread concerns about greenhouse gas emissions, particularly carbon dioxide.[73] Addressing CO_2 emissions is essential to combat climate change and ensure sustainable development. A key strategy to tackle this issue involves converting CO_2 into valuable chemicals and fuels using renewable, carbon-neutral energy sources; thus, facilitating the transition to a "low-carbon" economy.[74] Solar-driven photocatalysis, which directly converts sunlight into chemical energy, offers a sustainable and scalable solution for reducing CO_2 emissions.[75] This approach not only provides a sustainable and carbon-neutral method for energy production but also contributes to mitigating climate change.[76] Recently, artificial photosynthetic systems have emerged as advanced solutions for CO_2 conversion. These systems use solar energy to drive chemical reactions, potentially offering a cost-effective means for the large-scale production of fuels and chemicals.[77]

Although the CO_2 reduction reaction (CO_2RR) is still under development, it shows great potential for converting CO_2 into valuable products.[78] Carbon monoxide (CO), a notable product of CO_2RR, is especially valuable because it can be produced at low overpotentials with high selectivity.[79] However, optimizing

View Article Online
DOI: 10.1039/D4CC06655C

reaction kinetics and minimizing concurrent hydrogen evolution remain critical challenges for enhancing CO production. As the field progresses, developing molecular catalysts with high activity, selectivity, and durability is crucial.[80, 81] Two main strategies have emerged to advance molecular CO_2 reduction catalysis: i) modifying ligands to adjust the redox properties of metal centers, and ii) utilizing second coordination sphere effects, such as incorporating charged or hydrogen-bonding groups to improve CO_2 capture and conversion.

Regarding the first approach, which focuses on ligand modifications, Savéant and colleagues, in their seminal work, demonstrated that the introduction of electron-withdrawing and electron-donating groups to the periphery of the iron-porphyrin macrocycle significantly impacts electrocatalytic performance (Fig. 6a).[82] By incorporating penta-fluorinated electron-withdrawing units, two effects were observed: i) a more positive shift in the standard potential of the iron-porphyrin, and ii) a decrease in the catalytic rate constant, resulting in lower turnover frequency (TOF) values. Furthermore, Ott and co-workers illustrated that strategic ligand modifications can unlock unconventional catalytic pathways that operate at lower overpotentials. This was achieved by introducing a methyl group at the *ortho* position of a bipyridine ligand of a ruthenium-terpyridine-bipyridine catalyst (Fig. 6b).[83] In 2001, a series of iron complexes were synthesized and evaluated for their electrocatalytic efficiency. These iron complexes, based on 2,2′:6′,2″-terpyridine and methylated bis(2-pyridylmethyl)amine ligands, exhibited selective CO_2 reduction to CO at remarkably low overpotentials (Fig. 6c).[84] Additionally, McCrory and colleagues demonstrated that, in cobalt pyridyldiimine complexes, the effective overpotential is primarily governed by the redox potential of the ligand. By designing cobalt complexes with extended conjugation and incorporating electron-withdrawing groups, they achieved significant improvements in catalytic activity (Fig. 6d).[85]

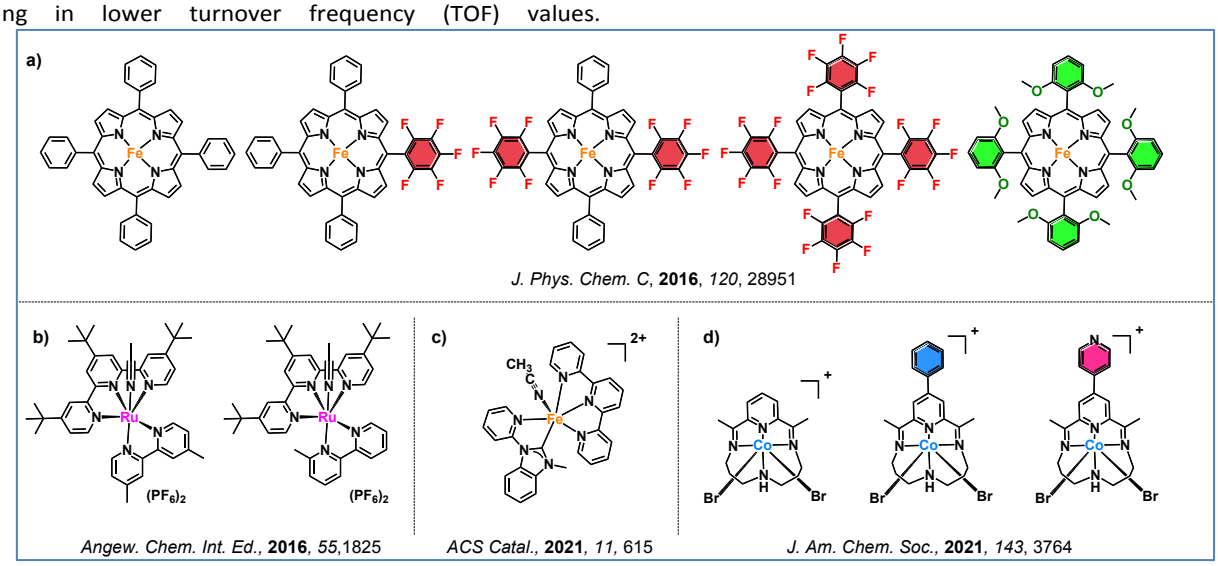

Fig. 6. Representative examples from the literature illustrating ligand modification strategies: a) introduction of electron-withdrawing groups to the iron-porphyrin macrocycle, b) strategic methylation of ruthenium-complexes in the ligand framework, c) iron-complex with modified ligands, and d) cobalt-complexes with extended conjugation and electron-withdrawing units.

Another effective strategy involves utilizing second coordination sphere effects, either through the incorporation of charged groups or the formation of hydrogen bonds. These modifications play a key role in enhancing CO_2 capture and conversion. The first example was presented in 2012 by Savéant and colleagues, who demonstrated that introducing 2,6-hydroxyphenyl groups at the periphery of an iron-porphyrin complex significantly enhanced catalytic activity (Fig. 7a).[86] This increased efficiency results from the high local proton concentration generated by the phenolic hydroxyl substituents, which enhance the catalytic activity. Further advances came in 2016, when the same research group introduced four positively charged trimethylanilinium groups into an iron-porphyrin, resulting in enhanced CO selectivity and stability (Fig. 7b).[87] The improved catalytic performance was driven by the coulombic interactions between the negatively charged Fe(0)-CO_2 adduct and the positively charged trimethylanilinium groups within the porphyrin macrocycle. Inspired by the active site of carbon monoxide dehydrogenase, Aukaullo, Halime, and coworkers functionalized iron-porphyrins with urea groups, which serve as multipoint hydrogen-bonding sites. These urea groups help stabilize CO_2 and promote its efficient reduction to CO (Fig. 7c).[88] They also explored the impact of atropisomerism, developing $\alpha\alpha$ and $\alpha\beta$ forms of the same urea-functionalized iron-porphyrin, demonstrating that the catalytic behavior is strongly influenced via the different hydrogen-bonding configurations.[89] Moreover, they discovered that multipoint hydrogen-bonding interactions might shift the redox activation from the commonly accepted Fe(0) state to the Fe(I) state, revealing new mechanistic insights into CO_2 reduction.[90] Chang and colleagues developed iron-porphyrins functionalized with imidazolium pendant units, which promoted synergistic effects through both positive charge and hydrogen-bond interactions (Fig. 7d).[91] This modification significantly enhanced both the

View Article Online
DOI: 10.1039/D4CC06655C

catalytic activity toward CO formation and CO_2 binding compared to non-functionalized iron-tetraphenyl porphyrin, which is widely used in CO_2 reduction studies.

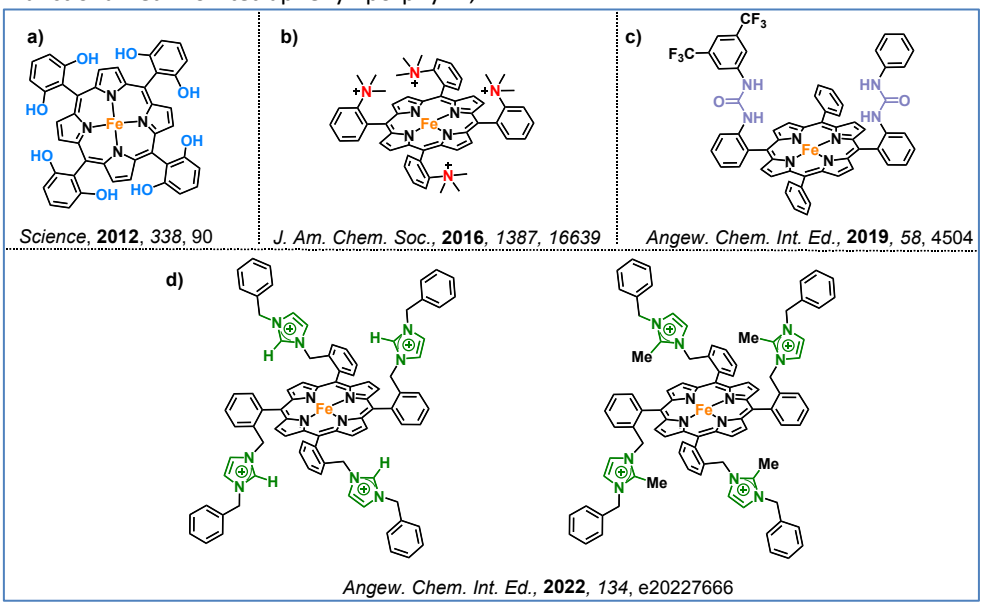

Fig. 7. Representative examples from the literature illustrating second coordination sphere effects: a) high local proton concentration facilitated by the phenolic hydroxyl substituents in porphyrins, b) positively charged trimethylanilinium groups into a porphyrin framework, c) urea groups help stabilize CO_2, and d) synergistic effects through both positive charge and hydrogen-bond interactions.

All the systems already discussed in this section focused on electrocatalytic CO_2 reduction, however our group has explored photocatalytic CO_2 reduction. We focused on developing a series of iron porphyrins, either covalently attached to a photosensitizer or used in combination with a photosensitizer in solution.[92, 93] In our recent work, we synthesized four modified iron porphyrins, each featuring distinct substitution patterns around the porphyrin core.[93] These structural variations had a significant impact on their catalytic performance in light-driven CO_2 reduction. The most efficient catalyst, **Fe-4F(TMA)-Por**, featured four fluorine atoms at the *ortho* and *meta* positions of the *meso*-phenyl groups and trimethylammonium groups (TMA) at the *para* positions (Fig. 8). This design enhanced the electron-withdrawing effects of the fluorine atoms and the CO_2 stabilization provided by the TMA groups, leading to an exceptionally high TON of 5500 and a TOF of 1375 h^{-1}. In contrast, **Fe-5F-Por**, which includes five fluorine atoms on each phenyl ring but lacks the ammonium groups, showed significantly lower activity. Although the electron-withdrawing fluorine atoms shifted the reduction potential, the absence of stabilizing cationic groups hindered CO_2 binding. This resulted in the lowest catalytic performance, with a TON of only 226. In another variation, **Fe-4F(DMA)-Por**, we replaced the trimethylammonium groups with dimethylamino groups (DMA). While the electron-withdrawing fluorine atoms still shifted the redox potential, the weaker CO_2 stabilization due to the lack of charged groups led to moderate performance (282 TONs). Finally, we prepared **Fe-TMA-Por**, which lacks fluorine atoms but retains the trimethylammonium groups at the *para* position of the phenyl rings. Although the positively charged groups improved CO_2 binding, the absence of fluorine limited electron transfer efficiency, resulting in a TON of 272. This work highlights the potential for developing more efficient molecular catalysts by tailoring their electronic and electrostatic properties. Our findings emphasize the critical balance between electron-withdrawing effects and CO_2 stabilization in optimizing photocatalytic performance. By fine-tuning this balance, a molecular catalyst can achieve both efficient charge transfer and enhanced CO_2 coordination.

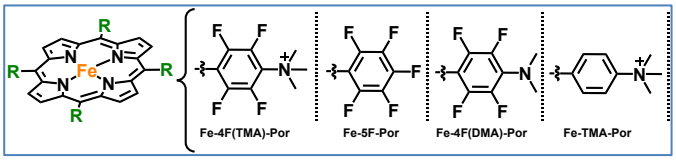

Fig. 8. The molecular structures of the iron-porphyrins studied in this work.[93]

In our second study, we developed and investigated a porphyrin-catalyst dyad specifically designed for photocatalytic CO_2 reduction.[92] The **FePor-Ru(bpy)** dyad was systematically evaluated against its individual components, namely an iron porphyrin (**FePor**) and a ruthenium trisbipyridine (**Ru(bpy)**), to assess the impact of their covalent attachment (Fig. 9). This covalent connection strategy was employed to mitigate diffusion limitations commonly encountered in multi-component systems and to facilitate rapid intermolecular electron transfer from the photosensitizer to the catalyst. The results demonstrated that the dyad exhibited superior catalytic activity compared to the photocatalytic system with the individual components (**FePor** and **Ru(bpy)**). This enhancement can be primarily attributed to the dyad's ability to facilitate faster electron transfer and more effective charge separation than the standalone components. Although the excited state of the photosensitizer is initially quenched within the dyad, the covalent linkage fosters the formation of catalytically active species at lower thermodynamic costs, which is crucial for

efficient CO_2 reduction. This interaction allows the dyad to initiate the catalytic cycle more effectively than when **FePor** and **Ru(bpy)** function independently. In summary, the dyad not only outperformed its individual components in terms of catalytic activity, but also revealed a unique mechanism that underscores the significance of covalent coupling. This study highlights the potential for designing hybrid systems that leverage the strengths of both components, ultimately leading to more effective strategies for CO_2 reduction.

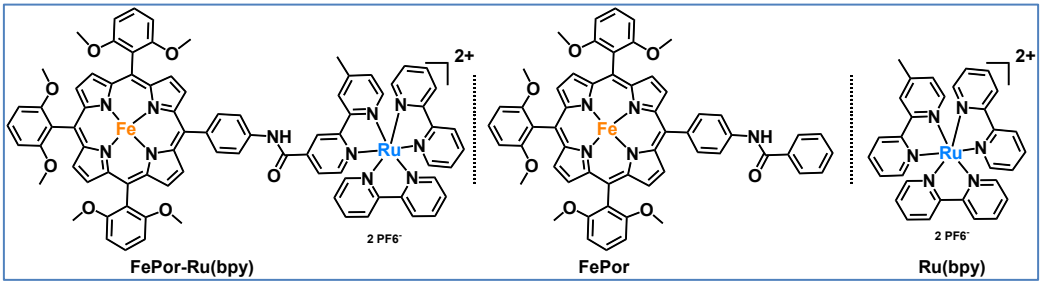

Fig. 9. Molecular structures of the photosensitizer-catalyst dyad (**FePor-Ru(bpy)**) and its individual components, the catalyst (**FePor**) and the photosensitizer (**Ru(bpy)**), as studied in this work.[92]

Apart from the reduction processes already covered in the previous two sections, the oxidative half reaction of water splitting plays a huge part in developing efficient biomimetic artificial photosynthetic systems. More specifically, due to water oxidation being a particularly challenging process, necessitating the simultaneous removal of four protons and electrons, several arrays have been studied targeting the photocatalytic oxygen evolution reaction, as discussed in the following section.

4. Photocatalytic water oxidation

The growing demand for renewable energy sources has increased the interest in water oxidation catalysis, a key reaction for sustainable energy production through water splitting.[94] Water oxidation to molecular oxygen constitutes the oxidative half-reaction of water splitting, which provides the necessary electrons and protons for the hydrogen generation reductive half-reaction. Solar-driven water oxidation mimics natural photosynthesis, providing a renewable and carbon-neutral approach for producing H_2 fuel, a clean and sustainable energy carrier.[95] Recent advancements in artificial photosynthetic systems have highlighted the potential of water oxidation catalysts (WOCs).[96] Notably, Sun and coworkers developed a molecular ruthenium catalyst for water oxidation that demonstrated activity similar to the oxygen-evolving complex of photosystem II in vivo, in terms of turnover frequency and stability.[97] However achieving high efficiency and durability remains challenging due to the energetically demanding nature of the oxygen evolution reaction (OER).[98] Current strategies to enhance water oxidation catalysis include: i) morphology modulation, atomic doping, and anchoring of single-atom catalysts,[99] ii) introduction of additional ligands and secondary coordination sphere interactions to facilitate the reaction kinetics.[100]

Porphyrins have attracted extensive attention in this field due to their bio-inspired design, mimicking chlorophylls in photosystem II. In water oxidation catalytic systems, porphyrins serve as ligands, stabilizing the WOC metal centers. They also facilitate multi-electron transfer processes essential for converting water (H_2O) into oxygen (O_2), protons (H^+), and electrons.[101-104] The porphyrin macrocycle offers both structural rigidity and electronic tunability, allowing for precise control over the redox properties of the central metal ion.[18] Metalloporphyrins with transition metals such as iron, manganese, nickel and cobalt can achieve the high oxidation states needed to form metal-oxo species, which are the active intermediates in OER.[105-107] Their macrocyclic ring also supports the stabilization of these high-valent species, preventing their decomposition and thus improving the overall catalytic efficiency.[108] Additionally, porphyrins can facilitate proton-coupled electron transfer (PCET), a key mechanism in water oxidation, by modulating the electronic environment around the metal center.[109, 110]

Inspired by the above, Bonnet and co-workers investigated hydrophilic nickel(II) porphyrins as catalysts for water oxidation in neutral to acidic conditions and in presence of $[Ru(bpy)_3]^{2+}$ as PS. They found that electron-poor substituents improved the catalytic efficiency by increasing the catalysts' oxidation potential. Ni-porphyrins with electron-deficient groups, like **Ni-3** and **Ni-4**, achieved 6-fold higher TOFs than electron-richer analogues **Ni-1** and **Ni-2** (Fig. 10a). However, the highly electron-poor **Ni-5**, was inactive since it presented an extremely high oxidation potential that the photosensitizer molecule $[Ru(bpy)_3]^{2+}$ was unable to achieve. Their electrochemical studies confirmed that electron-withdrawing substituents increased their oxidation potentials, balancing the driving force for water oxidation with electron transfer from the catalyst to the photosensitizer. **Ni-3** and **Ni-4** highlighted the potential of electron-tuned Ni-porphyrins to act as promising photocatalysts in OER, as they showcased both stability and catalytic activity.[102]

View Article Online
DOI: 10.1039/D4CC06655G

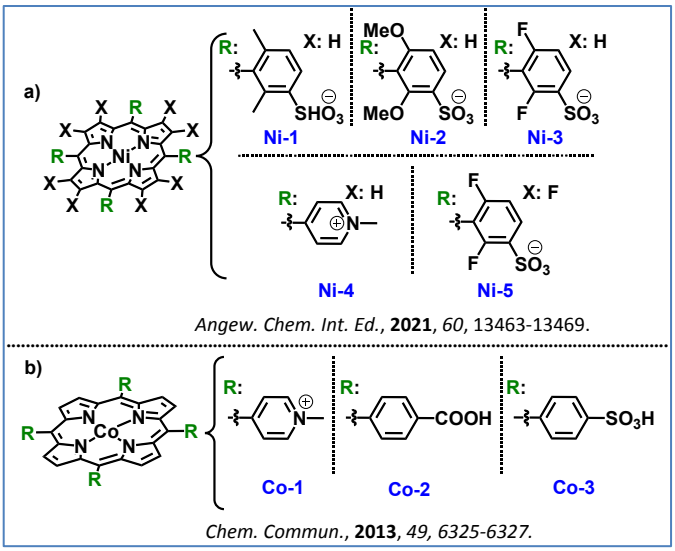

Fig. 10. Representative examples from the literature illustrating ligand modification strategies: a) hydrophilic Ni(II)-porphyrins with electron-withdrawing groups, b) water-soluble Co(II)-porphyrins with electron-withdrawing groups.

Another noble metal free set of porphyrins was investigated by Sakai and collaborators who applied water-soluble Co-porphyrins (**Co-1**, **Co-2**, **Co-3**, Fig. 10b) as WOCs. They tested those three catalysts in the presence of $Ru(bpy)_3^{2+}$ photosensitizer and sodium persulfate ($Na_2S_2O_8$) as sacrificial electron acceptor at pH 11, with **Co-3** presenting the highest activity. A second-order dependence on the catalyst concentration was observed in this work, suggesting that a bimolecular radical coupling step controls the reaction rate. Post-reaction analysis via ESI-MS indicated oxidative cleavage of the porphyrin ring, with oxidation products remaining bound to the cobalt center, ruling out cobalt nanoparticle formation.[42]

In an effort to prepare WOCs with increased stability, researchers have developed 2D and 3D materials that contain noble-metal free porphyrins. Paille et. al successfully developed a novel POM@MOF system, consisting of the porphyrinic MOF (photosensitizer) with an immobilized polyoxometalate catalyst, $[(PW_9O_{34})_2Co_4(H_2O)_2]^{10-}$, that presented high photocatalytic activity and stability (Fig. 11a). Computational studies revealed the role of TCPP porphyrin ligands in boosting oxidizing power and the MOF structure in stabilizing the catalytic site.[111] Notably, Wang and coworkers introduced an ionic-type 2D covalent organic framework (COF), **CoTPP-CoBpy$_3$**, that integrates cobalt porphyrin and cobalt bipyridine units to enhance photocatalytic water oxidation (Fig. 11b). This COF exhibits superior hydrophilicity and dispersibility, forming large nanosheets that facilitate local water collection at active sites. Key characteristics, including ultrafast charge transfer (1.8 ps) and prolonged charge-separated state (1.2 ns), support the efficient hole accumulation at CoTPP centers, achieving a high oxygen production rate of 7323 µmol·g^{-1}· h^{-1}.[112]

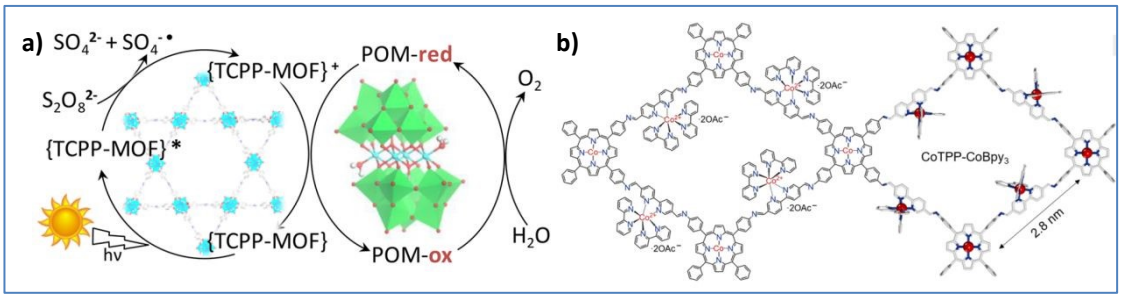

Fig. 11. a) Schematic illustration of the light-driven OER by $P_2W_{18}Co_4$@MOF-545. Reproduced from ref. 111 with permission from American Chemical Society, copyright 2018. b) Chemical structure of CoTPP-CoBpy$_3$ COF. Reproduced from ref. 112 with permission from American Association for the Advancement of Science, copyright 2024.

Having described homogenous and heterogenous photocatalytic systems for OER in the previous reports, we now turn our attention to analogous electrocatalytic systems. Han et. al applied the water-soluble cationic nickel(II) porphyrin **Ni-4** (Fig. 10a) as a molecular electrocatalyst for water oxidation in neutral aqueous conditions, achieving an onset potential of ~1.0 V (vs. NHE). **Ni-4** operated as a homogeneous electrocatalyst without forming NiOx films, exhibiting consistent activity across a broad pH range (2.0 - 8.0) and stability over 10 hours.[113] This example illustrates the potential of a single noble metal free porphyrin to act both as photo- and electro-catalyst for OER.[102, 113] In another report Wang et. al investigated a series of cationic cobalt porphyrins as WOC electrocatalysts (Fig. 12a), with **Co-4** demonstrating the highest efficiency in neutral aqueous conditions. This catalyst achieved an O_2 production rate of 170 nmol·cm^{-2}·min^{-1}, with a Faradaic efficiency close to 90%. Buffer bases with higher pKa values were found to lower the catalytic onset potential, suggesting critical role in proton-coupled electron transfer and O-O bond formation. The study confirmed **Co-4** robustness which showed no degradation or metal leaching over extended operation.[114]

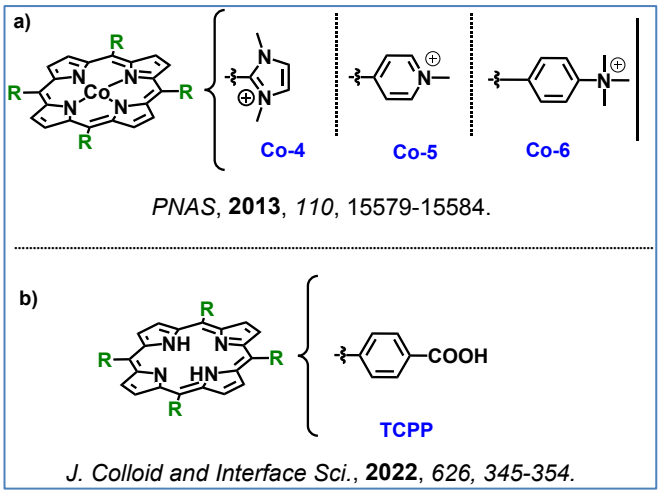

Fig. 12. a) Chemical structures of water-soluble Co(II)-porphyrins used as electrocatalysts for OER by Wang et al.,[114] b) Chemical structure of TCPP.

Recently, a promising approach to water oxidation catalysis has emerged, which integrates the beneficial aspects of both photocatalytic and electrocatalytic systems: the development of photoanodes for photo-electrocatalytic (PEC) oxygen evolution reaction. Towards this direction, Xie and coworkers developed a hybrid photoanode, CoPi/**TCPP**/Ti-Fe_2O_3, integrating Ti-doped hematite, a simple free base porphyrin (**TCPP**, Fig. 12b), and cobalt phosphate (CoPi) cocatalyst to enhance photocatalytic water oxidation. The strategic band alignment of Ti-Fe_2O_3, **TCPP**, and CoPi allows directional transfer of photogenerated holes from Ti-Fe_2O_3 to CoPi through **TCPP**; hence improving charge separation at the interface and facilitating efficient hole injection into the catalytic site. This design achieved a photocurrent density of 1.84 mA/cm^2 at 1.23 V vs. RHE, significantly outperforming CoPi/Ti-Fe_2O_3 alone. This study highlights the critical role of porphyrin in promoting charge transfer in photoanodes, offering a promising approach for designing efficient PEC systems for water oxidation.[115]

Inspired by the above reports and in alignment with the new PEC approach for water oxidation systems, our research team synthesized a molecular dyad comprising of a ruthenium tris(bipyridyl) photosensitizer coupled with a cost-effective nickel porphyrin catalyst (Fig. 13). The **NiP-Ru** dyad effectively combines light absorption and catalytic water oxidation functionalities, utilizing the Ru-complex as a light-harvester and Ni-porphyrin as the active water oxidation site. In initial experiments conducted in organic media, the covalently linked dyad demonstrated superior photocatalytic efficiency compared to a non-covalent, two-component system, as confirmed by the direct detection of O_2 via an optical oxygen sensor. Moving one step forward, we employed the **NiP-Ru** dyad in a photoelectrochemical cell, where it was immobilized on a TiO_2 photoanode via carboxylate anchoring groups. This work demonstrated a proof of concept, where the dyad-based PEC device performs visible light induced water oxidation in neutral aqueous media.[43]

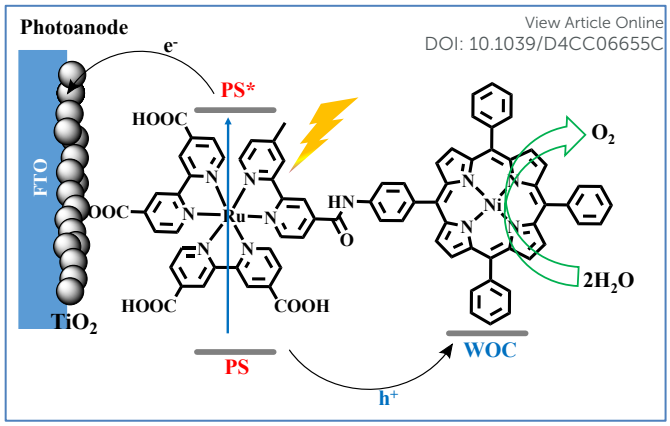

Fig. 13. Schematic illustration of the photo-electrocatalytic water oxidation by the NiP-Ru dyad photoanode. Reproduced from ref. 43 from Royal Society of Chemistry, copyright 2022.

5. Photocatalytic alcohol oxidation

The rapid expansion of global energy demand, coupled with escalating environmental concerns, has driven the search for sustainable and carbon-neutral energy solutions. Photocatalytic processes for H_2 generation and CO_2 reduction have garnered significant attention, offering the potential to both harness solar energy and contribute to a reduced carbon footprint.[5, 116] A central challenge in solar fuel photocatalytic systems, however, lies in efficiently managing the oxidative half-reactions occurring at the anode. Traditionally, the oxygen evolution reaction has been employed as the anodic counterpart to H_2 production or CO_2 reduction.[117] Nonetheless, OER presents several critical disadvantages that hinder its efficacy in photocatalytic and electrocatalytic systems. Primarily, OER suffers from sluggish kinetics, as it requires a four-electron transfer process to produce oxygen from water and additionally it requires high potential (1.23 V *vs*. NHE at pH = 0).[118] Furthermore, O_2 has low economic value and OER demands catalysts that can withstand harsh oxidative conditions, often necessitating the use of costly noble metals like iridium or ruthenium. Additionally, OER's production of oxygen introduces safety concerns due to the potential formation of explosive H_2/O_2 mixtures. These limitations make OER an energetically inefficient and economically challenging process.[119] Alternatively, to enhance H_2 evolution and CO_2 reduction rates, researchers often introduce co-catalysts and various SEDs (e.g., ascorbic acid, formic acid, triethylamine, triethanolamine, and lactic acid) as hole scavengers into the reaction system.[50] This approach leads to significant waste of resources but also results in the generation of by-products causing environmental pollution.[120]

Recognizing the challenges posed by the OER or the presence of SEDs, researchers have begun to explore alternative strategies for the anode reaction in photo-driven solar fuel production systems. The motivation behind this effort is not only to find a way to provide the necessary electrons and protons for the reductive half-reactions with lower anodic overpotential and more favorable kinetics, but also to find new means of

generating value-added chemical products via the oxidation reaction. In this regard, photocatalytic oxidation half-reactions such as biomass conversion, alcohol oxidation,[121] amine oxidation,[122] degradation of organic pollutants in wastewater,[123] photo-reforming of waste plastics,[124] and H_2O_2 production[120] have attracted great interest.

Among them, the selective oxidation of alcohols to carbonyl compounds is one promising approach since it generates higher-value products, requires a significantly lower potential and only two holes/photons instead of four.[125] Selective oxidation of alcohols is a crucial organic transformation with significant laboratory and industrial importance. The resulting carbonyl compounds (i.e., aldehydes and ketones) are valuable structural building blocks for the synthesis of pharmaceutical intermediates and fine chemicals.[126] For example, formaldehyde, benzyl aldehyde, and 4-methyl benzyl aldehyde are widely used in the fragrance, confectionery, beverage, and pharmaceutical industries. However, traditional chemical oxidation methods involve toxic and corrosive heavy-metal oxidants. Moreover, strong oxidants and harsh operating conditions are required that generate undesired and overoxidized products, and significant waste. Thus, light-driven alcohol oxidation offers a potentially appealing alternative that is more cost-effective, safer, and environmentally friendly. Moreover, alcohols are abundant feedstock since they can be extracted from biomass.[29] Therefore, the efficient conversion of alcohols to aldehydes or ketones via oxidant-free photocatalysis has attracted significant research attention.[125]

Various solar-driven H_2 evolving systems coupled with alcohol oxidation derivatives have been reported in the literature. Li *et al*. developed a hybrid photocatalytic system that employs graphitic carbon nitride (g-C_3N_4) as semiconductor, alongside a ruthenium complex and platinum as the oxidation and reduction catalysts, respectively. This system performed selective oxidation of benzyl alcohols coupled with H_2 evolution in pure water under visible light irradiation (Fig. 14a).[130] The selectivity of benzyl alcohols oxidation towards the corresponding benzaldehydes is significantly enhanced due to the formation of the active Ru(IV)=O intermediate species of the molecular catalyst, through efficient hole transfer from g-C_3N_4 to the Ru catalyst. Similarly, Reisner and co-workers reported a hybrid photocatalytic system composed of carbon nitride functionalized with cyanamide groups on its surface, paired with a molecular nickel(II) bis(diphosphine) catalyst.[131] This system effectively integrates light-driven hydrogen evolution reaction and benzylic alcohol oxidation (Fig. 14b). Under optimized conditions, the hybrid system exhibited high activity for both HER and aldehyde production, achieving a rate of 763 mmol g^{-1} h^{-1} and a quantum efficiency of 15%. The turnover frequency was calculated to be 76 h^{-1} based on the amount of nickel, with a conversion rate of 4-methylbenzyl alcohol reaching 83.0%. Transient absorption spectroscopy revealed that the cyanamide groups on the surface of carbon nitride suppressed electron-hole recombination, thereby enhancing catalytic efficiency. These groups helped suppress the recombination of excited electrons and holes, thereby increasing the overall yield. However, the system's operational lifetime was limited, likely due to the instability of the nickel catalyst under photocatalytic conditions.

Fig. 14. (a) Schematic representation of a redox system containing a molecular Ru catalyst and Pt modified g-C_3N_4 composite oxidizing benzyl alcohols to aldehydes with over 99% selectivity. Reproduced from ref. 130 with permission from Elsevier, copyright 2018. (b) Schematic

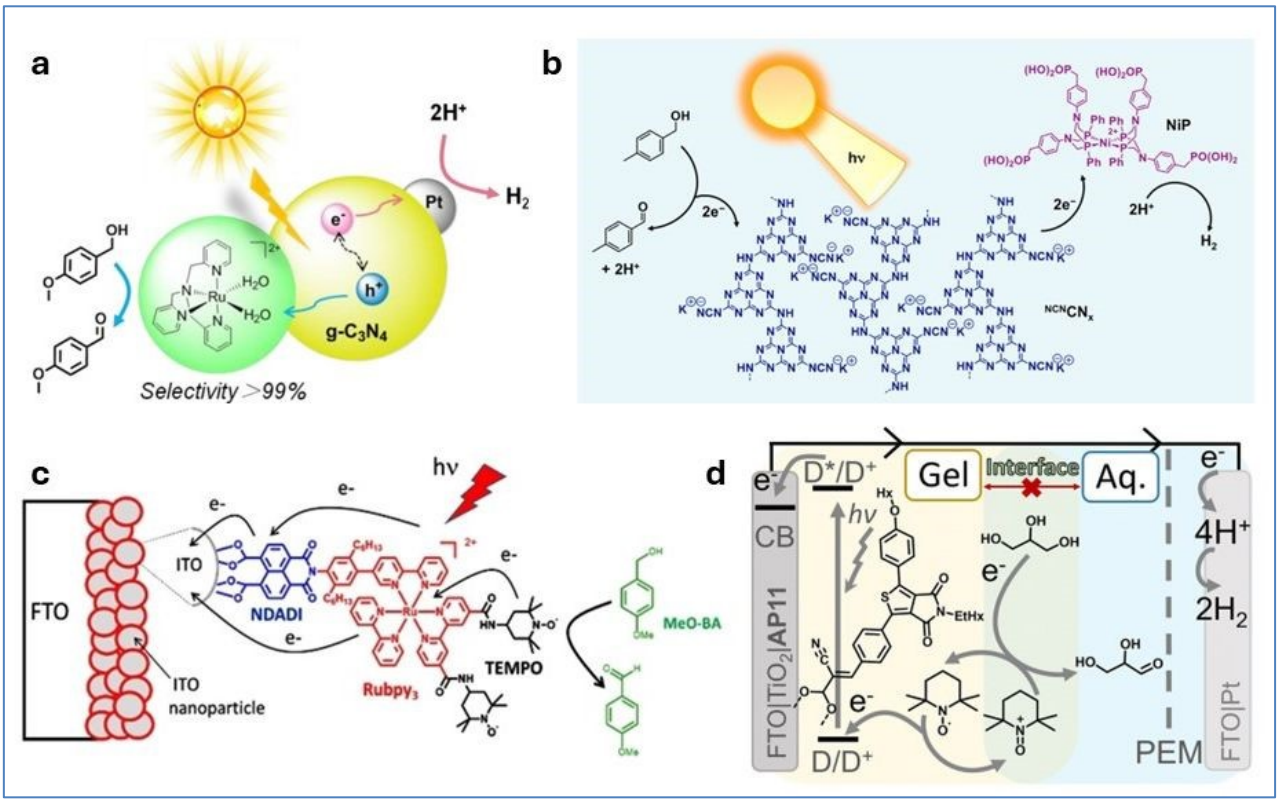

representation of a closed redox system for solar-driven H_2 evolution coupled with alcohol oxidation. Reproduced from ref. 131 with permission from American Chemical Society, copyright 2016. (c) Schematic representation of the photoanodic compartment for the NDADI–Ru-TEMPO triad supported onto ITO nanoparticles. Reproduced from ref. 132 with permission from John Wiley and Sons, copyright 2021. (d) Schematic representation of an aqueous biphasic DSPEC with a TEMPO containing redox-gel layer for glycerol oxidation. Reproduced from ref. 133 with permission from John Wiley and Sons, copyright 2022.

View Article Online DOI: 10.1039/D4CC06655G

Odobel and co-workers developed a hybrid photocatalytic system by immobilizing a molecular triad (**NDADI–Ru-TEMPO**) on a nano-ITO electrode.[132] The triad includes a Ru-tris-bipyridine complex as photosensitizer, linked to 2,2,6,6-tetramethyl-1-piperidine N-oxyl (TEMPO) as an alcohol oxidation catalyst, and naphthalenedicarboxyanhydride dicarboximide (NDADI) as an electron acceptor (Fig. 14c). Linear sweep voltammograms under chopped light irradiation in the presence of 50 mM para-methoxybenzyl alcohol, demonstrated an increased photocurrent response, reaching a net photocurrent of about 150–180 μA cm^{-2}. Under light irradiation and in pH 10 carbonate buffer, the triad achieved selective oxidation of para-methoxybenzyl alcohol to para-methoxybenzaldehyde with a TON of ~150 in 1 hour at a bias of 0.4 V *vs* SCE. Under optimal conditions, the average Faradaic efficiency was on the order of 80%. Nitroxides in general and TEMPO in particular are very active, cheap, green catalysts for alcohol oxidation,[134, 135] that are even applied to chemical industry.[136] Reek and co-workers developed an aqueous dye-sensitized photoelectrochemical cell (DSPEC) capable of oxidizing glycerol and at the same time produce H_2.[133] In this work a mesoporous TiO_2 electrode was sensitized with a thienopyrroledione-based organic dye and a TEMPO catalyst for glycerol oxidation (Fig. 14d). Both components were embedded in a 3 mm thick acetonitrile-based redox gel on the TiO_2 surface, creating a biphasic system with the aqueous solution. Under one-sun irradiation in a 0.1 M glycerol solution (pH 8.3), the cell achieved a photocurrent density near 200 μA cm^{-2} with nearly quantitative Faradaic efficiency for glyceraldehyde production, remaining stable for up to 48 hours. The introduction of the gel layer presented a 10-fold increase in the oxidation of glycerol compared to the aqueous system. This was attributed to the gel's ability of stabilizing the photoanode components from detachment under the alkaline conditions required for glycerol oxidation.

Our group explored the development of a TiO_2-based DSPEC for alcohol oxidation, using a TEMPO organo-catalyst covalently linked, for the first time, to a zinc porphyrin (ZnP) sensitizer.[137] Two different dyads (Fig. 15), each distinguished by the nature of the anchoring group (carboxylic acid *vs*. hydroxamic acid) attached to the porphyrin, were synthesized and their absorption, emission, and electrochemical characteristics were recorded. The photovoltaic properties of the dyads were initially tested in dye-sensitized solar cells (DSSCs) to optimize the dyeing conditions and assess their relative efficiencies. The TEMPO-substituted dyads outperformed the reference Zn-porphyrin without TEMPO, showing significantly higher short-circuit current (J_{sc}) and open-circuit voltage (V_{oc}). The incident photon-to-current conversion efficiency (IPCE) reached 2.6% at 430 nm, corresponding to the Soret absorption band. Then the SDPEC systems were effectively applied to the photoelectrochemical oxidation of benzyl alcohol derivatives. The optimal performance was observed in an aqueous borate buffer at pH 8, using the hydroxamic acid-anchored **hyd-ZnP-TEMPO** dyad. Under these conditions, para-methoxy benzaldehyde was selectively produced, achieving an average photocurrent density of 200 μA/cm^2, a Faradaic efficiency of 82%, a TON of 26, and a TOF of 47 h^{-1}. In acetonitrile, with N-methyl-imidazole as a base, the system is also active but with lower efficiency (photocurrent density ~100 μA/cm^2, Faradaic efficiency 76%, TON 13, TOF 24 h^{-1}). The reduced efficiency in acetonitrile was primarily due to photocatalyst leaching from the TiO_2 electrode, whereas in aqueous conditions, porphyrin degradation was the main factor limiting the catalytic performance. Transient absorption measurements revealed rapid electron injection from the excited Zn-porphyrin into the TiO_2 conduction band, forming a porphyrin radical cation. A slower electron transfer followed this from TEMPO to $ZnPor^+$, which partially competed with charge recombination. This observation was consistent with the low driving force (0.1 eV) and the weak electronic coupling between the two components. A comparison between the **hyd-ZnP-TEMPO** dyad and the bi-component system, "hyd-ZnP + ac-TEMPO", in acetonitrile showed that both systems offered similar performance. However, the covalent approach displayed easier catalyst recovery and required a smaller amount of catalyst. This photocatalytic system represents one of the most efficient systems ever reported for alcohol oxidation in DSPECs.

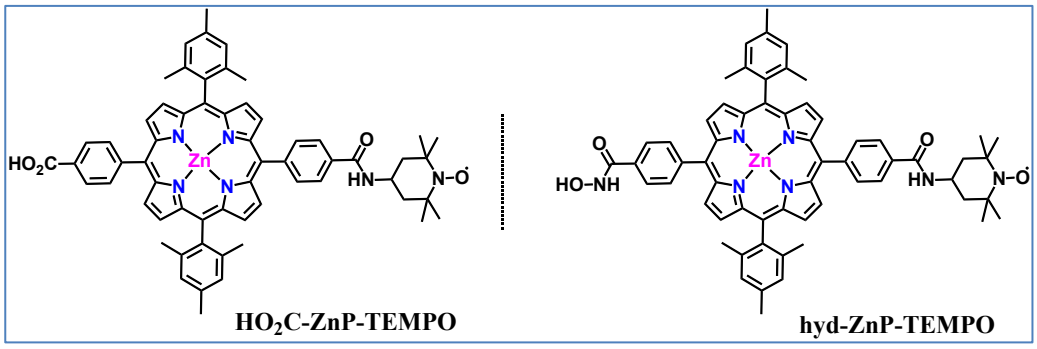

Fig. 15. Molecular structures of the two ZnP-TEMPO dyads that were used for the development of a TiO_2-based DSPEC.

View Article Online
DOI: 10.1039/D4CC06655C

FEATURE ARTICLE

In our team's most recent work, a dye-sensitized photocatalytic system was reported that enables simultaneous H_2 production and selective alcohol oxidation to aldehydes without using a SED.[138] DSP is an appealing photocatalytic system due to its simpler preparation process compared to DSPEC, which involves the additional steps of preparing electrodes, setting up wiring, and installing a membrane to separate the anolyte and catholyte. Traditionally, DSP systems are composed of a dye and a hydrogen evolution catalyst (HEC) co-grafted onto n-type semiconductor (n-SC) nanoparticles (NPs), such as TiO_2.[67] In most cases their activity relies on SEDs like ascorbic acid or triethanolamine to regenerate the oxidized dye, a process that is costly and environmentally unsustainable.[70] Here, a diketopyrrolopyrrole (DPP) dye covalently linked to a TEMPO-based catalyst replaces the SED, enabling the conversion of alcohols, such as benzyl alcohol and methoxybenzyl alcohol, to aldehydes while producing H_2 (Fig. 16). Under visible-light irradiation in the presence of platinum NPs as the HEC on TiO_2 nanoparticles, a TON of up to 50 for H_2 evolution was achieved along with the simultaneous conversion of alcohols into high-value aldehyde products. Reaction conditions such as pH, dye loading, and Pt concentration were optimized to maximize both H_2 and aldehyde production. The highest rate of H_2 evolution (200 $\mu mol \cdot h^{-1} \cdot g^{-1}$ of TiO_2) was observed at pH=8, with 24 nmol of **DPP-TEMPO** per mg of TiO_2 and with 3.2 nmol of Pt^0/mg of TiO_2. Furthermore, testing under sunlight simulation confirmed that the DSP system produces H_2 with a slightly lower TON of 27, verifying its functionality under real-world light conditions. Stability studies demonstrated that H_2 evolution ceases after approximately 4 hours of irradiation, primarily due to the photodecomposition of the DPP photosensitizer. In this setup, H_2 gas accumulates in the reaction headspace, while aldehydes remain in solution, facilitating product separation and enhancing the system's practicality for scalable applications. This approach has promising implications for sustainable photocatalytic systems, potentially extending to CO_2 or N_2 reduction, broadening the scope for DSPs without SEDs, and emphasizing renewable fuel and value-added product generation.

Fig. 16. Schematic representation of the dual-functional photocatalytic system based on a DPP dye covalently linked to the TEMPO catalyst. Reproduced from ref. 138 with permission from John Wiley and Sons, copyright 2024.

6. Outlook and Perspectives

Light-driven biomimetic catalysis is one of the most widely investigated concepts of artificial photosynthesis, due to its importance and resemblance to natural photosynthetic systems in generating and storing solar fuels. One of the main advantages of such systems, particularly water splitting and

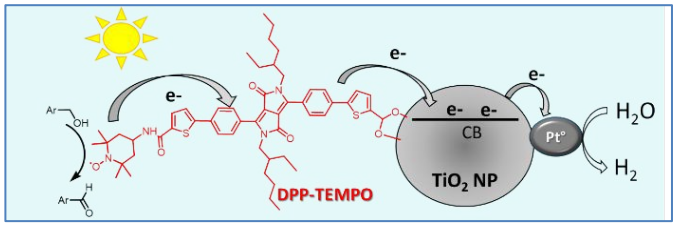

carbon dioxide reduction, relies on their versatility towards storing solar energy through fuel forming reactions with high value. A sustainable strategy that facilitates the transition to a "low-carbon" economy is the solar-driven photocatalytic transformation of carbon dioxide into useful and valuable chemicals and fuels. Additionally, though the reductive half reaction of artificial water splitting, H_2 is produced in a clean way and then gets stored for further use; hence facilitating both the exploitation and generation of green energy.

On the other hand, the oxidative half-reaction of water splitting, although an appealing process, is characterized by high energetic demands. Also, its main product (O_2) has very low commercial value and a high risk of generating harmful reactive species. Therefore, alternative oxidation reactions are commonly targeted for the anodic part of such artificial assemblies that can assist the reductive half-reaction while simultaneously generating value-added products. The most appealing approach is the photocatalytic oxidation of alcohols as they produce high-valued carbonyl compounds and serve as a sustainable environment remediation strategy.

In this Feature article we have highlighted the unique advantages of employing metalloporphyrins, both as photosensitizers and as catalysts, in developing sustainable and efficient biomimetic photocatalytic systems capable of producing solar fuels as well as offering solutions to environmental issues. By analyzing recent reports, we were able to display important advantages of metalloporphyrins, such as structural design, light-harvesting capability and charge separation efficiency, while also displaying limitations of porphyrin-based artificial photosynthetic assemblies. Notably, for each targeted catalytic process a few distinct strategies are discussed, emphasising some of the most important advancements. Our conceptual approach along with the results of our experimental work allowed us to understand important energetic requirements of each process. Moreover, optimal structural modifications of metalloporphyrins as well as the components and substrates, needed to construct highly efficient artificial photosynthetic systems, are identified. Specifically, our work on H_2 production systems reveals that the

most promising and efficient approach relies on heterogeneous photocatalysts. Such systems are formed by the adsorption of metalloporphyrins and/or co-catalysts onto semiconducting nanoparticles. Additionally, our targeted carbon dioxide reduction arrays demonstrated that structural fine-tuning leads to highly efficient Fe-porphyrin photocatalysts with favorable redox potentials and enhanced CO_2 coordination. However, the need for a sacrificial agent in the artificial photosynthetic assemblies described herein constitutes one of their main drawbacks. As a result, the most auspicious approach concerns the development of systems that combine efficient reductive photocatalysts that produce solar fuels, with oxidative co-catalysts that facilitate the simultaneous production of valuable chemicals and eliminate the use of detrimental sacrificial agents.

The first choice for such systems for the oxidative half-reaction would be O_2 evolving catalysts. Even so, as shown in this review, metalloporphyrins can act as water oxidation catalysts their low stability in the harsh conditions of OER systems, as well as their use in combination with noble metal-based complexes are important limitations. What is more, the product of this catalytic process has very low commercial value. For that reason, we highlight an alternative oxidative process; the solar-driven oxidation of alcohols. This reaction yields high-valued chemicals while providing the necessary electrons and protons for the reduction reaction. Therefore, we anticipate that the present article will aid in designing metalloporphyrin-based hybrid systems that combine components for the two half-reactions. Despite the promising efficiencies demonstrated in laboratory settings, translating metalloporphyrin-based photocatalytic systems into scalable and industrially viable technologies requires addressing a few challenges: material cost, catalyst regeneration, and integration into existing energy infrastructure. Emerging trends such as machine learning for catalyst optimization, tandem photocatalytic systems combining multiple reaction pathways, and hybrid organic-inorganic assemblies offer exciting avenues to enhance the performance and applicability of metalloporphyrin-based systems, paving the way for next-generation artificial photosynthesis technologies. Such biomimetic systems offer opportunities to serve as a more effective strategy for generating solar fuels and value-added chemicals in an environmentally friendly and sustainable manner.

Data availability

No primary research results, software or code have been included and no new data were generated or analysed as part of this review.

Conflicts of interest

"There are no conflicts to declare".

Acknowledgements

Dr. Emmanouil Nikoloudakis gratefully acknowledges the Bodossaki Foundation for financial support.

View Article Online
DOI: 10.1039/D4CC06655C

Notes and references

1. J. Min Park, J. H. Lee and W.-D. Jang, *Coord. Chem. Rev.*, 2020, **407**, 213157.
2. J. M. Park, K.-I. Hong, H. Lee and W.-D. Jang, *Acc. Chem. Res.*, 2021, **54**, 2249-2260.
3. Y. Shi, F. Zhang and R. J. Linhardt, *Dyes Pigments*, 2021, **188**, 109136.
4. S. Chen, J. Wei, X. Ren, K. Song, J. Sun, F. Bai and S. Tian, *Molecules*, 2023, **28**, 4283.
5. E. Nikoloudakis, I. López-Duarte, G. Charalambidis, K. Ladomenou, M. Ince and A. G. Coutsolelos, *Chem. Soc. Rev.*, 2022, **51**, 6965-7045.
6. M. K. Panda, K. Ladomenou and A. G. Coutsolelos, *Coord. Chem. Rev.*, 2012, **256**, 2601-2627.
7. Y. Kuramochi, Y. Fujisawa and A. Satake, *J. Am. Chem. Soc.*, 2020, **142**, 705-709.
8. S. Hiroto, Y. Miyake and H. Shinokubo, *Chem. Rev.*, 2017, **117**, 2910-3043.
9. M. O. Senge, *Chem. Commun.*, 2011, **47**, 1943-1960.
10. R. J. P. Williams, *Chem. Rev.*, 1956, **56**, 299-328.
11. M. O. Senge, S. A. MacGowan and J. M. O'Brien, *Chem. Commun.*, 2015, **51**, 17031-17063.
12. M. O. Senge, N. N. Sergeeva and K. J. Hale, *Chem. Soc. Rev.*, 2021, **50**, 4730-4789.
13. M. Tahoun, C. T. Gee, V. E. McCoy, P. M. Sander and C. E. Müller, *RSC Adv.*, 2021, **11**, 7552-7563.
14. V. Nikolaou, E. Nikoloudakis, K. Ladomenou, G. Charalambidis and A. G. Coutsolelos, *Front. Chem. Biol.*, 2024, **2**.
15. A. Khaledian and S. Zakavi, *Inorg. Chem. Commun.*, 2024, **167**, 112727.
16. A. G. Mojarrad and S. Zakavi, *Cat. Sci. Technol.*, 2018, **8**, 768-781.
17. K. Rybicka-Jasińska and D. Gryko, in *Photochemistry: Volume 49*, eds. S. Crespi and S. Protti, The Royal Society of Chemistry, 2021, vol. 49, p. 457-478.
18. R. Das, P. Kumar Verma and C. M. Nagaraja, *Coord. Chem. Rev.*, 2024, **514**, 215944.
19. N. S. Lewis and D. G. Nocera, *Proc. Natl. Acad. Sci.*, 2006, **103**, 15729-15735.
20. M. Đokić and H. S. Soo, *Chem. Commun.*, 2018, **54**, 6554-6572.
21. A. Kudo and Y. Miseki, *Chem. Soc. Rev.*, 2009, **38**, 253-278.
22. K. Ladomenou, M. Natali, E. Iengo, G. Charalampidis, F. Scandola and A. G. Coutsolelos, *Coord. Chem. Rev.*, 2015, **304**, 38-54.
23. A. J. Esswein and D. G. Nocera, *Chem. Rev.*, 2007, **107**, 4022-4047.
24. T. Inoue, A. Fujishima, S. Konishi and K. Honda, *Nature*, 1979, **277**, 637-638.
25. S. Xie, Q. Zhang, G. Liu and Y. Wang, *Chem. Commun.*, 2016, **52**, 35-59.
26. M. W. Kanan and D. G. Nocera, *Science*, 2008, **321**, 1072-1075.
27. M. D. Kärkäs, E. V. Johnston, O. Verho and B. Åkermark, *Acc. Chem. Res.*, 2014, **47**, 100-111.

28. C. R. Lhermitte and K. Sivula, *ACS Catal.*, 2019, **9**, 2007-2017.
29. L. I. Granone, F. Sieland, N. Zheng, R. Dillert and D. W. Bahnemann, *Green Chem.*, 2018, **20**, 1169-1192.
30. J. S. O'Neill, L. Kearney, M. P. Brandon and M. T. Pryce, *Coord. Chem. Rev.*, 2022, **467**, 214599.
31. N. Chanda, D. Koteshwar, S. Gonuguntla, S. Bojja, U. Pal and L. Giribabu, *Mater. Adv.*, 2021, **2**, 4762-4771.
32. A. Vidal, F. Adamo, E. Iengo and E. Alessio, *Inorg. Chim. Acta*, 2021, **516**, 120143.
33. H. Yuan, Y. Yu, S. Yang, Q. Lei, Z. Yang, B. Lan and Z. Han, *Chem. Commun.*, 2024, **60**, 6292-6295.
34. T. Nagasawa, S. I. Allakhverdiev, Y. Kimura and T. Nagata, *Photochem. Photobiol. Sci.*, 2009, **8**, 174-180.
35. A. Charisiadis, E. Giannoudis, Z. Pournara, A. Kosma, V. Nikolaou, G. Charalambidis, V. Artero, M. Chavarot-Kerlidou and A. G. Coutsolelos, *Eur. J. Inorg. Chem.*, 2021, **2021**, 1122-1129.
36. G. Di Carlo, C. Albanese, A. Molinari, S. Carli, R. Argazzi, A. Minguzzi, F. Tessore, E. Marchini and S. Caramori, *ACS Appl. Mater. Interfaces*, 2024, **16**, 14864-14882.
37. Y. Dong, R. Nie, J. Wang, X. Yu, P. Tu, J. Chen and H. Jing, *Chin. J. Catal.*, 2019, **40**, 1222-1230.
38. M. Yamamoto, L. Wang, F. Li, T. Fukushima, K. Tanaka, L. Sun and H. Imahori, *Chem. Sci.*, 2016, **7**, 1430-1439.
39. F. D'Souza and O. Ito, *Chem. Commun.*, 2009, 4913-4928.
40. V. Nikolaou, A. Charisiadis, C. Stangel, G. Charalambidis and A. G. Coutsolelos, *C*, 2019, **5**(3), 57.
41. P. Gotico, Z. Halime and A. Aukauloo, *Dalton Trans.*, 2020, **49**, 2381-2396.
42. T. Nakazono, A. R. Parent and K. Sakai, *Chem. Commun.*, 2013, **49**, 6325-6327.
43. E. Nikoloudakis, A. Z. Alsaleh, G. Charalambidis, A. G. Coutsolelos and F. D'Souza, *Chem. Commun.*, 2022, **58**, 12078-12081.
44. D. G. Nocera, *Acc. Chem. Res.*, 2012, **45**, 767-776.
45. D. Gust, T. A. Moore and A. L. Moore, *Acc. Chem. Res.*, 2009, **42**, 1890-1898.
46. T. Keijer, T. Bouwens, J. Hessels and Joost N. H. Reek, *Chem. Sci.*, 2021, **12**, 50-70.
47. R. J. Cogdell, T. H. P. Brotosudarmo, A. T. Gardiner, P. M. Sanchez and L. Cronin, *Biofuels*, 2010, **1**, 861-876.
48. J. Barber and P. D. Tran, *J. R. Soc. Interface*, 2013, **10**, 20120984.
49. I. Holmes-Gentle, S. Tembhurne, C. Suter and S. Haussener, *Nat. Energy*, 2023, **8**, 586-596.
50. K. Ladomenou, M. Natali, E. Iengo, G. Charalampidis, F. Scandola and A. G. Coutsolelos, *Coord. Chem. Rev.*, 2015, **304-305**, 38-54.
51. L. Wang, H. Fan and F. Bai, *MRS Bull.*, 2020, **45**, 49-56.
52. N. Queyriaux, R. T. Jane, J. Massin, V. Artero and M. Chavarot-Kerlidou, *Coord. Chem. Rev.*, 2015, **304-305**, 3-19.
53. E. Nikoloudakis, A. G. Coutsolelos and E. Stratakis, *Energ. Fuel*, 2024, **38**, 19222-19235.
54. A. Sartorel, M. Bonchio, S. Campagna and F. Scandola, *Chem. Soc. Rev.*, 2013, **42**, 2262-2280.
55. P. D. Tran, V. Artero and M. Fontecave, *Energy Environ. Sci.*, 2010, **3**, 727-747.
56. P. Du and R. Eisenberg, *Energy Environ. Sci.*, 2012, **5**, 6012-6021.
57. N. Coutard, N. Kaeffer and V. Artero, *Chem. Commun.*, 2016, **52**, 13728-13748. View Article Online DOI: 10.1039/D4CC06655C
58. T. Lazarides, M. Delor, I. V. Sazanovich, T. M. McCormick, I. Georgakaki, G. Charalambidis, J. A. Weinstein and A. G. Coutsolelos, *Chem. Commun.*, 2014, **50**, 521-523.
59. A. Panagiotopoulos, K. Ladomenou, D. Sun, V. Artero and A. G. Coutsolelos, *Dalton Trans.*, 2016, **45**, 6732-6738.
60. M.-Y. Yeh, T.-Y. Tseng, H.-C. Hsieh, B.-X. Wu, Y.-S. Liao, Y.-C. Yeh and J.-C. Liu, *ChemPhotoChem*, 2020, **4**, 481-486.
61. Y. Liu, H. Wang, S. Li, C. Chen, L. Xu, P. Huang, F. Liu, Y. Su, M. Qi, C. Yu and Y. Zhou, *Nat. Commun.*, 2020, **11**, 1724.
62. M. Kownacki, S. M. Langenegger, S.-X. Liu and R. Häner, *Angew. Chem. Int. Ed.*, 2019, **58**, 751-755.
63. E. Nikoloudakis, K. Karikis, J. Han, C. Kokotidou, A. Charisiadis, F. Folias, A. M. Douvas, A. Mitraki, G. Charalambidis, X. Yan and A. G. Coutsolelos, *Nanoscale*, 2019, **11**, 3557-3566.
64. V. Nikolaou, G. Charalambidis and A. G. Coutsolelos, *Chem. Commun.*, 2021, **57**, 4055-4058.
65. R. Cao, G. Wang, X. Ren, P.-C. Duan, L. Wang, Y. Li, X. Chen, R. Zhu, Y. Jia and F. Bai, *Nano Lett.*, 2022, **22**, 157-163.
66. E. Orfanos, K. Ladomenou, P. Angaridis and A. G. Coutsolelos, *Dalton Trans.*, 2022, **51**, 8009-8014.
67. J. Willkomm, K. L. Orchard, A. Reynal, E. Pastor, J. R. Durrant and E. Reisner, *Chem. Soc. Rev.*, 2016, **45**, 9-23.
68. S. Rajak, N.-N. Vu, P. Kaur, A. Duong and P. Nguyen-Tri, *Coord. Chem. Rev.*, 2022, **456**, 214375.
69. L. Zani, M. Melchionna, T. Montini and P. Fornasiero, *J. Phys. Energy*, 2021, **3**, 031001.
70. J.-F. Huang, Y. Lei, T. Luo and J.-M. Liu, *ChemSusChem*, 2020, **13**, 5863-5895.
71. V. Nikolaou, G. Charalambidis, K. Ladomenou, E. Nikoloudakis, C. Drivas, I. Vamvasakis, S. Panagiotakis, G. Landrou, E. Agapaki, C. Stangel, C. Henkel, J. Joseph, G. Armatas, M. Vasilopoulou, S. Kennou, D. M. Guldi and A. G. Coutsolelos, *ChemSusChem*, 2021, **14**, 961-970.
72. V. Nikolaou, E. Agapaki, E. Nikoloudakis, K. Achilleos, K. Ladomenou, G. Charalambidis, E. Triantafyllou and A. G. Coutsolelos, *Chem. Commun.*, 2023, **59**, 11256-11259.
73. J. Du, D. Xiang, K. Zhou, L. Wang, J. Yu, H. Xia, L. Zhao, H. Liu and W. Zhou, *Nano Energy*, 2022, **104**, 107875.
74. T. R. Knutson, R. Zhang and L. W. Horowitz, *Nature Commun.*, 2016, **7**, 13676.
75. M. Gao, T. Zhang and G. W. Ho, *Nano Res.*, 2022, **15**, 9985-10005.
76. M. Robert, *ACS Energy Lett.*, 2016, **1**, 281-282.
77. C. Fu, Z. Wan, X. Yang, J. Zhang and Z. Zhang, *J. Mater. Chem. A*, 2024, **12**, 28618-28657.
78. S. R. Lingampalli, M. M. Ayyub and C. N. R. Rao, *ACS Omega*, 2017, **2**, 2740-2748.
79. E. O. Eren and S. Özkar, *J. Power Sources*, 2021, **506**, 230215.
80. E. Boutin, L. Merakeb, B. Ma, B. Boudy, M. Wang, J. Bonin, E. Anxolabéhère-Mallart and M. Robert, *Chem. Soc. Rev.*, 2020, **49**, 5772-5809.
81. A. R. Groves, *Nat. Synth.*, 2024, **3**, 556-556.
82. I. Azcarate, C. Costentin, M. Robert and J.-M. Savéant, *J. Phys. Chem. C*, 2016, **120**, 28951-28960.
83. B. A. Johnson, S. Maji, H. Agarwala, T. A. White, E. Mijangos and S. Ott, *Angew. Chem. Int. Ed.*, 2016, **55**, 1825-1829.
84. S. Gonell, J. Lloret-Fillol and A. J. M. Miller, *ACS Catal.*, 2021, **11**, 615-626.

85. W. Nie, D. E. Tarnopol and C. C. L. McCrory, *J. Am. Chem. Soc.*, 2021, **143**, 3764-3778.
86. C. Costentin, S. Drouet, M. Robert and J. M. Savéant, *Science*, 2012, **338**, 90-94.
87. I. Azcarate, C. Costentin, M. Robert and J.-M. Savéant, *J. Am. Chem. Soc.*, 2016, **138**, 16639-16644.
88. P. Gotico, B. Boitrel, R. Guillot, M. Sircoglou, A. Quaranta, Z. Halime, W. Leibl and A. Aukauloo, *Angew. Chem. Int. Ed.*, 2019, **58**, 4504-4509.
89. P. Gotico, L. Roupnel, R. Guillot, M. Sircoglou, W. Leibl, Z. Halime and A. Aukauloo, *Angew. Chem. Int. Ed.*, 2020, **59**, 22451-22455.
90. S. Amanullah, P. Gotico, M. Sircoglou, W. Leibl, M. J. Llansola-Portoles, T. Tibiletti, A. Quaranta, Z. Halime and A. Aukauloo, *Angew. Chem. Int. Ed.*, 2024, **63**, e202314439.
91. M. R. Narouz, P. De La Torre, L. An and C. J. Chang, *Angew. Chem. Int. Ed.*, 2022, **61**, e202207666.
92. T. Adelais, G. Philipp, H. Christian, H.-T. Minh-Huong, P. Thomas, L. Winfried, C. Georgios, C. Athanassios, H. Zakaria and A. Ally, *C. R. Chim.*, 2021, **24**, 101-114.
93. A. Stoumpidi, A. Trapali, M. Poisson, A. Barrozo, S. Bertaina, M. Orio, G. Charalambidis and A. G. Coutsolelos, *ChemCatChem*, 2023, **15**, e202200856.
94. S. Dash, A. S. K, J. S, V. H. W. D, E. D, S. K. Surapraraju and S. K. Natarajan, *Int. J. Hydrog. Energy*, 2024, **83**, 614-629.
95. Z. A. K. Khattak, H. A. Younus, N. Ahmad, M. Alomar, H. Ullah, M. Al-Abri, R. Al-Hajri, C.-M. Kao and F. Verpoort, *Int. J. Hydrog. Energy*, 2024, **76**, 141-151.
96. S. Ye, C. Ding and C. Li, in *Advances in Inorganic Chemistry*, eds. R. van Eldik and C. D. Hubbard, Academic Press, 2019, vol. 74, pp. 3-59.
97. L. Duan, F. Bozoglian, S. Mandal, B. Stewart, T. Privalov, A. Llobet and L. Sun, *Nat. Chem.*, 2012, **4**, 418-423.
98. F. Creazzo and S. Luber, *Chem. Eur. J.*, 2021, **27**, 17024-17037.
99. Y. Xie, F. Luo and Z. Yang, *Energy Rev.*, 2024, **3**, 100103.
100. T. Liu, L. Fan, H. Yang, L. Wang, X. Fan and L. Sun, *Artif. Photosynth.*, 2024, **1**, 14-26.
101. A. K. Singh and L. Roy, *ACS Omega*, 2024, **9**, 9886-9920.
102. C. Liu, D. van den Bos, B. den Hartog, D. van der Meij, A. Ramakrishnan and S. Bonnet, *Angew. Chem. Int. Ed.*, 2021, **60**, 13463-13469.
103. X. Wu, F. Li, B. Zhang and L. Sun, *J. Photochem. Photobiol. C: Photochem. Rev.*, 2015, **25**, 71-89.
104. J. Meng, P. Bi, J. Jia, X. Sun and R. Chen, *ChemistrySelect*, 2017, **2**, 4882-4888.
105. S. Fukuzumi, T. Kojima, Y.-M. Lee and W. Nam, *Coord. Chem. Rev.*, 2017, **333**, 44-56.
106. W. Lai, R. Cao, G. Dong, S. Shaik, J. Yao and H. Chen, *J. Phys. Chem. Lett.*, 2012, **3**, 2315-2319.
107. Y. Naruta, M.-a. Sasayama and T. Sasaki, *Angew. Chem. Int. Ed. in English*, 1994, **33**, 1839-1841.
108. B. Yao, Y. He, S. Wang, H. Sun and X. Liu, *Int. J. Mol. Sci.*, 2022, **23**, 6036.
109. J. Rosenthal and D. G. Nocera, *Acc. Chem. Res.*, 2007, **40**, 543-553.
110. C. J. Gagliardi, A. K. Vannucci, J. J. Concepcion, Z. Chen and T. J. Meyer, *Energy Environ. Sci.*, 2012, **5**, 7704-7717.
111. G. Paille, M. Gomez-Mingot, C. Roch-Marchal, B. Lassalle-Kaiser, P. Mialane, M. Fontecave, C. Mellot-Draznieks and A. Dolbecq, *J. Am. Chem. Soc.*, 2018, **140**, 3613-3618.
112. E. Zhou, X. Zhang, L. Zhu, E. Chai, J. Chen, J. Li, D. Yuan, L. Kang, Q. Sun and Y. Wang, *Sci. Adv.*, 2024, **10**, eadk8564.
113. Y. Han, Y. Wu, W. Lai and R. Cao, *Inorg. Chem.*, 2015, **54**, 5604-5613.
114. D. Wang and J. T. Groves, *Proc. Natl. Acad. Sci.*, 2013, **110**, 15579-15584.
115. Q. Bu, X. Liu, Q. Zhao, G. Lu, X. Zhu, Q. Liu and T. Xie, *J. Colloid Interface Sci.*, 2022, **626**, 345-354.
116. Z. Wang, J. Fan, B. Cheng, J. Yu and J. Xu, *Mater. Today Phys.*, 2020, **15**, 100279.
117. B. Zhang and L. Sun, *Chem. Soc. Rev.*, 2019, **48**, 2216-2264.
118. F. Wang and S. S. Stahl, *Acc. Chem. Res.*, 2020, **53**, 561-574.
119. X. Liang, X. Cao, W. Sun and Y. Ding, *ChemCatChem*, 2019, **11**, 6190-6202.
120. H. Liu, S. He, J. Qu, Y. Cai, X. Yang, C. M. Li and J. Hu, *Chin. J. Catal.*, 2024, **65**, 1-39.
121. B. You, G. Han and Y. Sun, *Chem. Commun.*, 2018, **54**, 5943-5955.
122. X. Bao, M. Liu, Z. Wang, D. Dai, P. Wang, H. Cheng, Y. Liu, Z. Zheng, Y. Dai and B. Huang, *ACS Catal.*, 2022, **12**, 1919-1929.
123. Y. Wu, X. Chen, J. Cao, Y. Zhu, W. Yuan, Z. Hu, Z. Ao, G. W. Brudvig, F. Tian, J. C. Yu and C. Li, *Appl. Catal. B: Environ.*, 2022, **303**, 120878.
124. T. Uekert, H. Kasap and E. Reisner, *J. Am. Chem. Soc.*, 2019, **141**, 15201-15210.
125. D. Tang, G. Lu, Z. Shen, Y. Hu, L. Yao, B. Li, G. Zhao, B. Peng and X. Huang, *J. Energy Chem.*, 2023, **77**, 80-118.
126. M.-Y. Qi, M. Conte, M. Anpo, Z.-R. Tang and Y.-J. Xu, *Chem. Rev.*, 2021, **121**, 13051-13085.
127. H. G. Cha and K.-S. Choi, *Nat. Chem.*, 2015, **7**, 328-333.
128. S. Kampouri and K. C. Stylianou, *ACS Catal.*, 2019, **9**, 4247-4270.
129. Q. Chen, Y. Liu, B. Mao, Z. Wu, W. Yan, D. Zhang, Q. Li, H. Huang, Z. Kang and W. Shi, *Adv. Funct. Mater.*, 2023, **33**, 2305318.
130. F. Li, Y. Wang, J. Du, Y. Zhu, C. Xu and L. Sun, *Appl. Catal. B: Environ.*, 2018, **225**, 258-263.
131. H. Kasap, C. A. Caputo, B. C. M. Martindale, R. Godin, V. W.-h. Lau, B. V. Lotsch, J. R. Durrant and E. Reisner, *J. Am. Chem. Soc.*, 2016, **138**, 9183-9192.
132. P. B. Pati, M. Abdellah, S. Diring, L. Hammarström and F. Odobel, *ChemSusChem*, 2021, **14**, 2902-2913.
133. D. F. Bruggeman, A. A. H. Laporte, R. J. Detz, S. Mathew and J. N. H. Reek, *Angew. Chem. Int. Ed.*, 2022, **61**, e202200175.
134. J. E. Nutting, M. Rafiee and S. S. Stahl, *Chem. Rev.*, 2018, **118**, 4834-4885.
135. F. Huang, F. Zhang, Y. Wang and X. Lang, *Trends Chem.*, 2024, **6**, 115-127.
136. R. Ciriminna and M. Pagliaro, *Org. Process Res. Dev.*, 2010, **14**, 245-251.
137. E. Nikoloudakis, P. B. Pati, G. Charalambidis, D. S. Budkina, S. Diring, A. Planchat, D. Jacquemin, E. Vauthey, A. G. Coutsolelos and F. Odobel, *ACS Catal.*, 2021, **11**, 12075-12086.
138. D. Romito, C. Govind, V. Nikolaou, R. J. Fernández-Terán, A. Stoumpidi, E. Agapaki, G. Charalambidis, S. Diring, E. Vauthey, A. G. Coutsolelos and F. Odobel, *Angew. Chem. Int. Ed.*, 2024, **63**, e202318868.

View Article Online
DOI: 10.1039/D4CC06655C

- No primary research results, software or code have been included and no new data were generated or analysed as part of this review.